Regional-Scale Impacts of Fluid Composition and Geologic Structure for Injection-Induced Seismicity in the Southern U.S. Midcontinent

Graydon Leo Konzen

Thesis submitted to the faculty of the Virginia Polytechnic Institute and State University in partial fulfillment of the requirements for the degree of

Master of Science
In
Geosciences

Ryan M. Pollyea
Martin C. Chapman
John A. Chermak

May 14, 2020
Blacksburg, Virginia

Keywords: Hydrogeology, Numerical Groundwater Modeling, Induced Seismicity, Geographic Information Systems

Regional-Scale Impacts of Fluid Composition and Geologic Structure for Injection-Induced Seismicity in the Southern U.S. Midcontinent

Graydon Leo Konzen

ABSTRACT

Over the last decade, an increase in earthquake occurrence in Oklahoma and Kansas has been linked to oilfield wastewater injection disposal, particularly into the regionally underpressured Arbuckle Group. The Arbuckle is hydraulically connected to Precambrian basement through an extensive fracture system, which transmits pressure perturbations from wastewater injections to seismogenic depths. Previous studies have convincingly attributed induced seismicity to pore pressure diffusion and solid elastic stressing, both resulting from fluid waste injection. Recent work adds to the physical understanding of injection-induced seismicity by demonstrating that the density differential between injection fluids and formation brines may also drive fluid pressure into the seismogenic basement. In this thesis, variable density groundwater flow is modeled in a numerical simulation comprising parts of the Anadarko Basin, the Anadarko Shelf, the Cherokee Platform, and the Nemaha Fault Zone as well as injection data from 2006-2018. Results show buoyancy forces interacting with regional stratigraphic dip to force density-driven pressure transients into the deep Anadarko Basin, aligning with previously unexplained earthquakes in that region.

Regional-Scale Impacts of Fluid Composition and Geologic Structure for Injection-Induced Seismicity in the Southern U.S. Midcontinent

Graydon Leo Konzen

GENERAL AUDIENCE ABSTRACT

Increased earthquake activity in Oklahoma and Kansas over the last decade is linked waste disposal related to hydrofracking. Oil and gas produced in the fracking process is often mixed with large amounts of water that is too salty to be used for public or industrial purposes. This water is disposed of via injection into deep geologic formations, which are rock layers in the upper portions of the Earth's crust. Waste water injections increase pressure conditions in these rocks, triggering earthquakes where none have been historically observed. Previous studies examining this phenomenon assume that the rock layers of the crust lie flat and level; simplify the nature of major faults, or cracks, in the crust; and do not consider differences in water chemistry between injected water and water that already occupies the crust. The study developed in this thesis considers the effect of these three factors with regard to how they influence the extent of the linkage between waste water injection and earthquakes in Oklahoma and Kansas. Results show that increased pressure aligns with earthquakes in an area of southwest Oklahoma that have not been explained by previous studies.

ACKNOWLEDGEMENTS

This study would not be possible without the support of my fellow graduate students and the Geosciences faculty at Virginia Tech. Special thanks to my adviser, Ryan M. Pollyea, and my committee members, Martin M. Chapman and John A. Chermak, for their expertise and guidance, and to my lab mates, Richard Jayne, Wu Hao, and Cameron Chambers for their collaboration and shared passion. Thanks are also due to Jonathan Prouty, whose sound technical advice helped to propel this work through some challenging issues. The facilities at Virginia Tech Advanced Research Computing made possible the numerical modeling performed herein. USGS grant #G19AP00011 provided funding for this study.

TABLE OF CONTENTS

INTRODUCTION

Induced seismicity is defined as earthquake activity that can be linked to human engineering activities (Ellsworth, 2013). Seismicity induced by fluid injection into geologic reservoirs was first noticed in the mid-1960s, when a single well was injecting hazardous fluid waste directly into Precambrian basement at the Rocky Mountain Arsenal facility near Denver, CO (Healy et al., 1968). Soon after injection began, people in the Denver area began reporting earthquakes where none had been felt since the late 19th century (Healy et al., 1968). Gutenberg-Richter analysis of the Denver earthquake sequence found an unnaturally high frequency of M4+ earthquakes, which propagated away from the injection well along a linear, northwest-propagating trend suggesting that the earthquakes were occurring along a pre-existing fault (Healy et al., 1968). Healy et al. (1968) contends that pore pressure disturbance alone is not enough to initiate seismic activity because tectonic stress conditions cause rocks to be stressed almost to their breaking strength. An important observation is that after injection stopped in early 1966, pore pressure rapidly recovered in the vicinity of the well but continued to expand into the far field (Healy et al., 1968). Moreover, earthquakes continued post-injection, with the largest occurring during this period (Healy et al., 1968).

Following the Denver earthquake sequence, Raleigh et al. (1976) proposed the hypothesis that wastewater injections cause earthquakes by increasing fluid pressure, which decreases effective stress on pre-existing faults. This hypothesis was tested at the Rangely, Colorado oilfield site by alternating deep fluid injections and subsequent withdrawals. Combining field data from the Rangely experiments with numerical simulations provided compelling evidence that Mohr-Coulomb failure theory explains injection-induced seismicity (Raleigh et al., 1976). Mohr-Coulomb theory states that

$$\tau = \tau_o + \mu\sigma_n \ (1)$$

where, τ is shear stress at failure, τ_o is the cohesive strength (considered to be nil on pre-existing faults), μ is the coefficient of friction, and σ_n is effective normal stress. In Equation 2, σ_n is calculated as,

$$\sigma_n = S_n - P_f \ (2)$$

where, S_n is the total normal stress acting inwards across a fault plane and P_f is pore fluid pressure acting outward and against S_n (Healy et al., 1968; Raleigh et al., 1976; Horton, 2012; Ellsworth, 2013). According to Equation 2, addition of fluids via injection can reduce σ_n to the point where τ is exceeded (Healy, 1968; Raleigh et al., 1976; Ellsworth, 2013). Since fluid cannot accumulate shear stress, such pore pressure elevation reduces effective normal stress, and if the shear stress acting parallel to a fracture trend is greater than the product of the effective normal stress and the rock's coefficient of friction, slip will occur (Raleigh et al., 1976; Ellsworth, 2013). Townend & Zoback (2000) showed that the shallow crust in intraplate settings is generally close to failure and constrained bulk permeability over 1 to 10 km scales in these settings to 10^{-14} – 10^{-17} m^2. This study also argues that ubiquitous faulting maintains the strength of the shallow (brittle) crust because the permeable fault zones keep pore fluid pressure at near-hydrostatic (Townend & Zoback, 2000). This combination of critically-stressed faults and near-hydrostatic fluid pressure suggests that small changes in pore pressure ≤ 0.1 MPa may be sufficient to trigger earthquakes (Reasenberg & Simpson, 1992; Townend & Zoback, 2000).

Since 2008, earthquake frequency throughout the central and eastern United States (CEUS) increased contemporaneously with unconventional oil and gas production (Ellsworth, 2013; Pollyea et al., 2018). As a result, there has been a commensurate increase in produced oilfield brine, defined as aqueous fluid with a total dissolved solids (TDS) concentration of ≥35,000 mg/L

(ppm). Unable to be economically treated for beneficial use, this brine is disposed of via injection into deep geologic formations (Ellsworth, 2013; Keranen et al., 2014; Murray, 2015; Pollyea et al., 2018; Rottmann, 2018). Throughout the CEUS, geologic fluid injection doubled from 1997 to 2013, with the vast majority of injection volume accounted for by saltwater disposal (SWD) as opposed to enhanced oil recovery (EOR) via water-flooding into pre-developed reservoirs (Walsh et al., 2015). Furthermore, the vast majority of SWD fluid is formation brine produced from unconventional plays as opposed to flowback water used in the fracking process (Walsh et al., 2015).

Many studies linking injection disposal to increased earthquake activity in the CEUS have focused on establishing spatiotemporal relationships between relocated earthquakes and injection wells (Ake et al., 2005; Holland, 2011; Frolich, 2011; Horton, 2012; Kim, 2013; Weingarten et al., 2015). Kim (2013) used 1-D seismic velocity modeling, regional waveform inversion, double-difference relocation, and Green's function analysis to locate the 2011-2012 Youngstown, OH earthquake swarm in Precambrian basement beneath a single injection well. Horton (2012) establishes a similar connection in the Arkoma Basin of west-central Arkansas, where five wells injecting into Paleozoic strata overlying Precambrian basement caused a ~150-fold increase in earthquakes between 2009 and 2011. This study also estimated the transmissivity and storage coefficient of fractured, crystalline basement to calculate pore overpressure transients exceeding 0.1 MPa at distances up to 20 km from an injection well (Horton, 2012). Horton (2012) also points out that it is not necessary for injected fluid itself to enter a fault zone to cause slip; instead, only injection-induced pressure transients need to enter a fault zone. Weingarten et al. (2015) uses a bootstrap resampling method to establish correlation between SWD injection rates and earthquakes but does not find such a relationship between cumulative injected volume or wellhead pressure

and earthquakes. Many seismological studies of induced earthquakes show that the strongest shocks in triggered earthquake sequences often occur months to years after injections are halted (Healy et al., 1968; Ake et al., 2005; Horton, 2012; Kim, 2013; Langenbruch et al., 2016). Furthermore, these earlier works suggest pressure disturbance distances of up to 20 km from injection wells. More recent studies report correlation distances between injection wells and seismicity exceeding ~70 km from clusters of high-rate injection wells, particularly in northern Oklahoma (Pollyea et al., 2018; Peterie et al., 2018; Langenbruch et al., 2018). In contrast, others highlight areas of seismic quiescence between earthquake swarms, which are attributed to differing fault orientations as well as aseismic slip and poroelastic stress transfer initiated by injection-induced pressure transients (Gugliemi et al., 2015; Yeck et al., 2016; Goebel et al., 2017).

Induced Seismicity in Oklahoma and Kansas

Over the last decade, anthropogenic earthquake activity due to subsurface disposal of oilfield wastewater has been most prevalent in Oklahoma and Kansas (Elsworth, 2013; Weingarten et al., 2015; Pollyea et al., 2018; Peterie et al., 2018). Induced seismicity in Oklahoma was first recognized by Holland (2013), who suggested a possible link between earthquakes and the rapid proliferation of unconventional petroleum production by hydraulic reservoir stimulation, which is colloquially known as "fracking." McNamara et al. (2015) found that sub-vertical to vertical strike-slip faults optimally oriented to regional tectonic stress field were responsible for over 3,500 earthquakes that occurred in Oklahoma between 2009 and 2014. Furthermore, most of these earthquake hypocenters are at $\leq$ 6 km depth in the upper crystalline basement, with the 5 - 6 km interval as the most frequent hypocentral depth (McNamara et al., 2015). Concentration of earthquakes along critically stressed faults occurring contemporaneously with widespread, high-volume saltwater disposal (SWD) suggests a causal relationship between the two according to

effective stress theory. It is now known with reasonable certainty that induced seismicity in Oklahoma and Kansas is not in response to the fracking process itself, but instead due to large-scale SWD into the Arbuckle Group (Keranen et al., 2013; 2014; Walsh et al., 2015; McNamara et al., 2015; Weingarten et al., 2015; Yeck et al., 2016; Langenbruch et al., 2016; 2018; Pollyea et al., 2018; 2019). Pressure disturbances are likely transmitted to seismogenic depths via a fracture network that provides a hydraulic connection between the Arbuckle Group and Precambrian basement (Rottmann, 2018, Pollyea et al., 2019).

Oklahoma seismicity records from 1974 to 2008 show a diffuse pattern of earthquake occurrence, with an average of one $M_w \geq 3$ event occurring annually (Walsh et al., 2015). Beginning in 2009, earthquakes of similar magnitude rapidly increase in frequency to over 100 in both 2013 and 2014, with epicenters clustered around injection wells (Walsh et al., 2015). Oklahoma seismicity peaked at 900× qits pre-2008 frequency in 2015 (Pollyea et al., 2018). The largest recorded earthquakes in Oklahoma to-date are the 2011 M_w 5.7 event near Prague and the 2016 M_w 5.8 event near Pawnee, both likely triggered by fluid injection (Langenbruch et al., 2018). Seismicity linked to SWD began to spread from Oklahoma into southeastern Kansas in 2013 (Walsh et al., 2015; Rubinstein et al., 2018; Peterie et al., 2018), with the largest to-date being a Mw 4.9 earthquake near Milan, KS in November 2014 (Norbeck & Rubinstein, 2018). Earthquake activity began decreasing in Oklahoma in 2016, possibly due to a combination of reduction in oil and gas prices and newly instituted regulation on injection disposal (Langenbruch et al., 2018; Pollyea et al., 2018; 2019). A number of seismology-based studies have predicted a decrease in earthquakes with decreased injection (Langenbruch et al., 2016; Norbeck & Rubinstein, 2018); however, seismicity in the region was still at least ~75× its historic levels in 2019 (OGS Statewide

Seismic Network) and significant events still occur, including the M_w 4.5 shock near Hutchinson, KS in January 2020 (USGS ComCat).

Keranen et al. (2014) conducted the first numerical groundwater modeling study linking pore pressure migration to seismicity in Oklahoma. This study shows that simulated pore pressure propagation from 89 injection wells in southcentral Oklahoma reasonably matches earthquake hypocenter locations leading up to the 2008 – 2012 Jones earthquake swarm (Keranen et al., 2014). Moreover, this work shows that just four 4 high-rate injectors, operating at combined 640,000 m^3 per month (4,000,000 bbl/mo) in the southeast Oklahoma City area, are responsible for most of the modeled pressure increase and thus seismicity (Keranen et al., 2014). Induced earthquakes occurred at distances of up to 35 km from these wells (Keranen et al., 2014) with a critical earthquake-triggering stress of ~0.07 MPa, which is consistent with previous evaluations of the static stress change required to induce earthquakes (Reasenberg & Simson, 1992; Townend & Zoback, 2000). More recently, Langenbruch et al. (2018) coupled numerical groundwater modeling and probabilistic earthquake hazard calculations to produce a regional seismicity forecast in north-central Oklahoma and southeastern Kansas through 2020. Using best-fit Arbuckle and basement permeabilities of 1×10^{-12} m^2 and 2×10^{-15} m^2, respectively, Arbuckle injections from 2000 to 2020 are modeled with a constant post-2018 injection rate to evaluate pore pressure disturbance (Langenbruch et al., 2018). Rates of pressure increase are then used to inform a modified Gutenberg-Richter analysis, ultimately predicting that seismic hazard will steadily decrease into the future, albeit with persistent, nonzero risk of damaging earthquakes (Langenbruch et al., 2018). Both Keranen et al. (2014) and Langenbruch et al. (2018) make two critical assumptions in hydrogeologic modeling: (1) geologic strata are of uniform thickness and

horizontal throughout and (2) both basement fluids and oilfield wastewater are of identical and constant density throughout the injection process.

Study Objectives

The objective of this study is to evaluate the role of fluid composition and regional-scale geologic structure on the spatial and temporal progression of fluid pressure transients caused by oilfield wastewater disposal. Regional-scale groundwater flow is influenced by geologic structure, such as surface topography, sedimentation patterns and tectonic deformation (Tóth, 1963; Downing et al., 1987; Bense et al., 2013; Ferguson et al., 2018). Additionally, fluid density has also been shown to be a major controlling factor in groundwater flow and is often subject to regional-scale variation (Osborn et al., 2013; Ferguson et al., 2018). In the context of oilfield wastewater disposal, Pollyea et al. (2019) found that oilfield wastewater in northern Oklahoma is characterized by much higher TDS concentrations (~200,000 ppm) than host rock fluids in the seismogenic basement (~100,000 ppm) (Blondes et al., 2018; Pollyea et al., 2019). This difference in TDS implies a significant fluid density differential, where higher TDS corresponds to higher density (Pollyea et al., 2019). Injecting high density wastewater results in the advective transport of high-density wastewater, which (i) displaces lower-density native brine, (ii) pushes pressure transients deeper and (iii) allows them to persist longer than constant density models predict (Pollyea et al., 2019). As a consequence, the combination of regional-scale structural gradients and high-density wastewater may cause density-driven pressure transients to migrate down-dip (Ferguson et al., 2018), which in turn causes earthquakes to become deeper and potentially higher magnitude (Pollyea et al., 2019). The study developed in this thesis builds upon the physical concepts established by Pollyea at al. (2019; 2020) to examine how regional-scale geologic structure will influence the spatiotemporal behavior of injection-induced fluid pressure transients

when compositional difference between wastewater and basement fluids are considered. I develop a regional-scale, numerical groundwater model of ~120,000 km^2 in north-central Oklahoma and southeastern Kansas (Fig. 1) to show that (1) the density differential between higher TDS injected fluid and lower TDS native brines and (2) complex structure, including fault zone permeability anisotropy and regional stratigraphic dip result in persistent overpressure conditions that align with deep-basin earthquakes previously unlinked to SWD.

Study Area and Geologic Setting

The study area encompasses an approximately 120,000 km^2 area of north-central Oklahoma (OK) and southeastern Kansas (KS), including the major cities of Tulsa and Oklahoma City, OK and Wichita, KS (Fig. 1). This region has a long history of oil and gas production (Higley, 2014) owing to prominent geologic features, including extensive fault zones and basin environments (Johnson, 2008; 1988). Parts of the Anadarko Basin, the Anadarko Shelf, the Cherokee Platform, and the Nemaha Fault Zone (NFZ) are included in this area (Zeller et al., 1968; Johnson, 1988; 2008; Northcutt & Campbell, 1995). The southern and eastern margins of the study area are bounded by the Wichita, Arbuckle, and Ouachita Mountains and the Ozark Plateau (Johnson, 1988; 2008). The north-south trending NFZ extends from Oklahoma City to northeastern Nebraska and bifurcates the study area into eastern and western halves (Zeller et al., 1968; Gay, 2003, McBee, 2003). The Anadarko Basin and the Anadarko Shelf occur in the western half of the study area, extend to the north into the Hugoton embayment of Kansas, Colorado and Texas, and are truncated by the Cimarron Arch and Amarillo Uplift to the west (Johnson, 2008). The eastern half of the study area comprises the Cherokee Platform (Johnson, 2008).

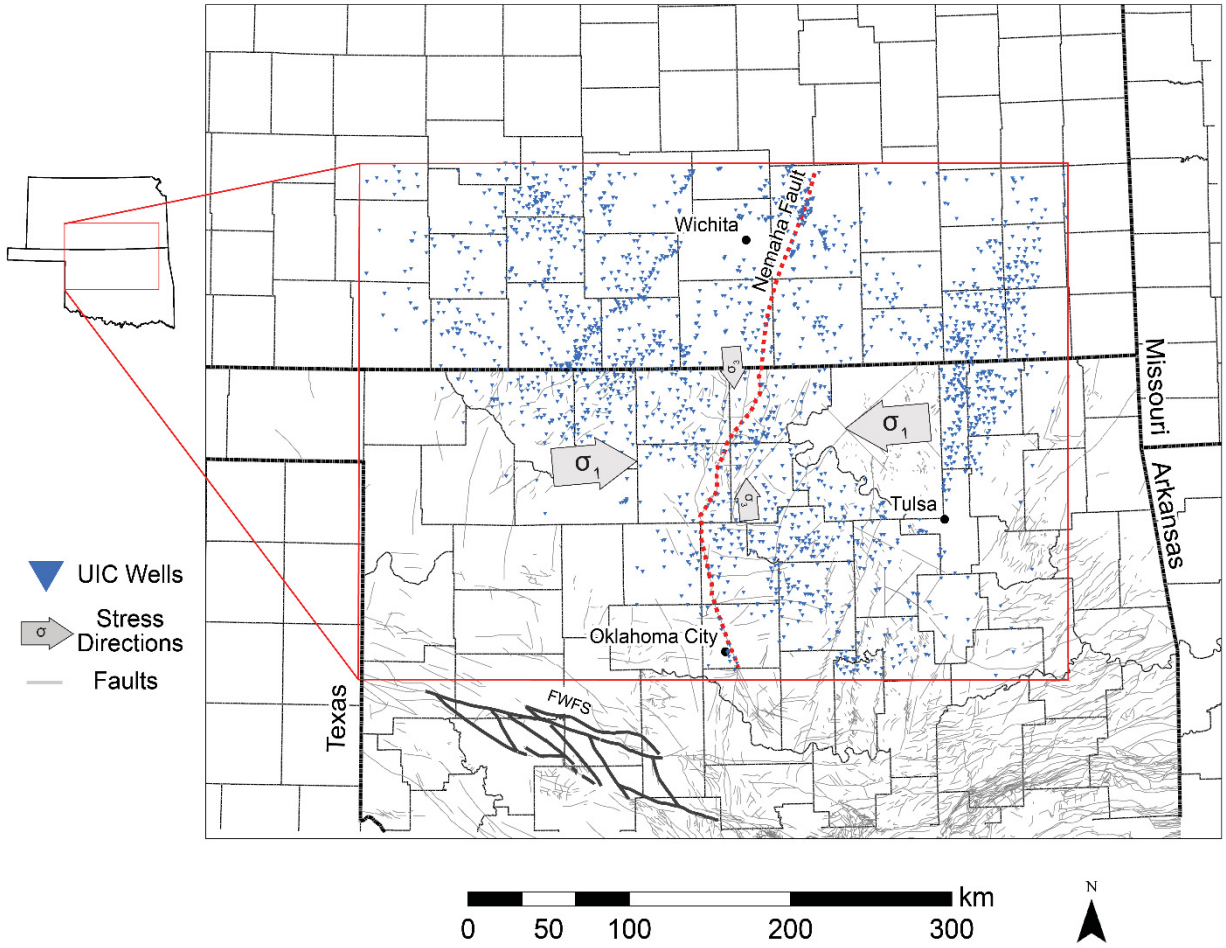

Figure 1: Map showing extent of study area in Oklahoma and Kansas with UIC wells active 2006 - 2018 (OCC Oil and Gas Well Database, KGS Fluid Injection Database), principal tectonic stress directions (Alt & Zoback 2017), and mapped faults in Oklahoma (Marsh & Holland 2015). Nemaha Fault Zone (NFZ) shown in red dashes; major faults in Frontal Wichita Fault System (FWFS) interpreted after Crone & Luza (1990) in bold gray. Horizontal orientation of maximum stress (σ_1) and minimum stress (σ_3) indicate strike-slip faulting regime.

The present geologic configuration of the region (Fig. 2) results from both tectonic and sedimentary processes beginning in the Precambrian (Zeller et al., 1968; Johnson, 1988; 2008; Northcutt & Campbell, 1995; Gay, 2003; McBee, 2003). Precambrian basement in Oklahoma and Kansas comprises igneous and metamorphic rock that is up to 1.4 billion years old (Zeller et al., 1968; Johnson, 2008). Oklahoma's basement also includes some Cambrian igneous and metamorphic rock in southern parts of the state (Johnson, 2008). In Oklahoma, the depth to basement ranges from 300 m below ground surface in the northeast to greater than 10,000 m in the

deepest part of the Anadarko Basin (Johnson, 1988; 2008). In Kansas, the top of basement ranges from ~200 m depth in the northeastern Nemaha Uplift to ~3,000 m depth in the southwest (Zeller et al., 1968). Basement exposures exist in the Wichita and Arbuckle mountains (Johnson, 2008).

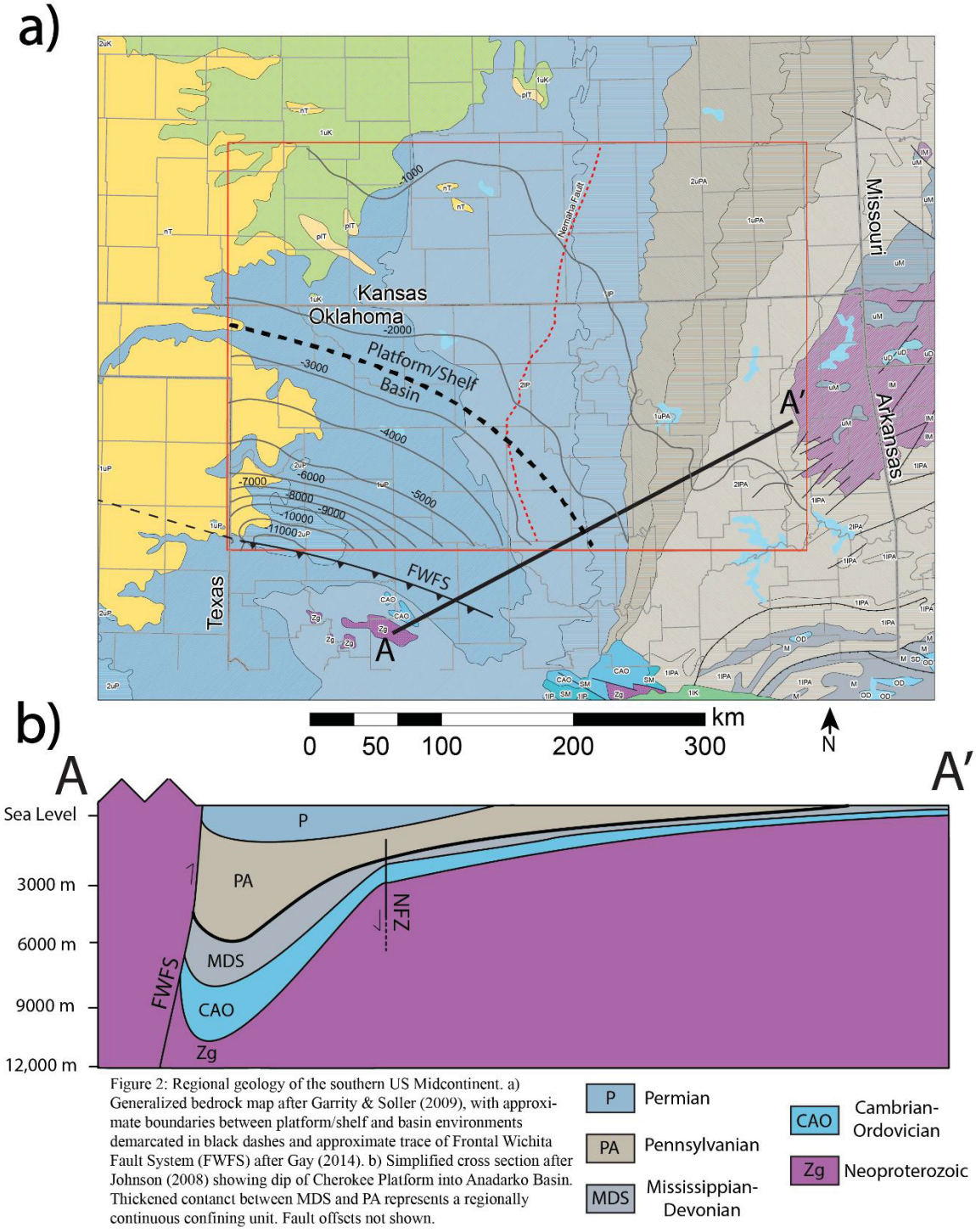

Figure 2: Regional geology of the southern US Midcontinent. a) Generalized bedrock map after Garrity & Soller (2009), with approximate boundaries between platform/shelf and basin environments demarcated in black dashes and approximate trace of Frontal Wichita Fault System (FWFS) after Gay (2014). b) Simplified cross section after Johnson (2008) showing dip of Cherokee Platform into Anadarko Basin. Thickened contanct between MDS and PA represents a regionally continuous confining unit. Fault offsets not shown.

Before early Paleozoic seas inundated Oklahoma and Kansas, extensive erosion and faulting removed Precambrian sediment leaving the basement erosional surface highly fractured (Rottmann, 2018). Deposition of the stratigraphically equivalent late Cambrian Reagan and Lamotte Sandstones created an unconformity on the basement and represents the first time in the geologic record that shallow seas inundated the US Midcontinent (Zeller et al., 1968; Johnson, 2008). These basal sandstones grade upwards into a thick section composed predominantly of dolomite (Zeller et al., 1968; Rottman, 2018; Johnson, 2008), herein called the Arbuckle Group or Arbuckle Formation. The late Cambrian to early Ordovician Arbuckle Group, largely limestone and dolomite, overlies the Reagan Sandstone in isolated areas and sits directly on top of basement virtually everywhere else in Oklahoma (Johnson, 2008). The Arbuckle overlies the Lamotte Sandstone over most of its extent in Kansas (Zeller et al., 1968). Both the Reagan and Lamotte Sandstones are of insignificant thicknesses at the regional scale (Zeller et al., 1968; Johnson, 2008). In small, isolated areas, a carbonate unit similar to and possibly part of the Arbuckle is the "Bonterre Dolomite" (Zeller et al., 1968; Franseen et al., 2004), which directly overlies basement rock; the Bonterre is herein included in the Arbuckle Group. The Arbuckle is roughly 600 m thick in Oklahoma's deepest basins (Johnson, 2008) and grades into or is truncated by younger units in central and northern Kansas (Zeller et al., 1968). In isolated areas, the Arbuckle is relatively thin or nonexistent due to relief of erosional basement features (Rottmann, 2018).

In order of stratigraphic succession from oldest to youngest, the remaining Ordovician record in Oklahoma consists mostly of Simpson Group Sandstones, Viola Group Limestones, and Sylvan Shale, which are together up to ~800 m thick in Oklahoma's deep basins (Johnson, 2008). Only part of Oklahoma's Simpson and Viola Groups exist in Kansas, achieving their maximum thicknesses in the south of the state and pinching out to the north and west (Zeller et al., 1968).

The late Ordovician Maquoketa Shale of Kansas is generally considered to be equivalent to the Sylvan Shale of Oklahoma (Zeller et al., 1968). Overlying Ordovician sediments in Oklahoma are the Silurian to Devonian limestones and shales of the Hunton Group, which are up to 300 m thick (Johnson, 2008). In Kansas, the Hunton Group is mostly restricted to the northeast (Zeller et al., 1968), and only occurs in the northernmost portion of the study area (Zeller et al., 1968). Overlying the Hunton Group is the Devonian Woodford Shale, the latter of which is up to 200 m thick in the Arbuckle Mountains (Johnson, 2008). Late Devonian to early Mississipian shale, called the Chattanooga Shale, also exists in Kansas throughout most of the study area (Zeller et al., 1968). Both the Woodford and the Chattanooga Shales are separated from underlying sediments by an angular unconformity (Rottmann, 2018; Johnson, 2008; Zeller et al., 1968).

Early to Middle Mississippian sediments in Oklahoma are predominantly limestone, with Sycamore Limestone in the south and Mississippi Lime in the north continuing into Kansas (Zeller et al., 1968; Johnson, 2008). Rapid subsidence of Oklahoma's southern basins in the latter half of the Mississippian left a thick sequence of mostly shale (Johnson, 2008). In the Ardmore Basin and the eastern Anadarko Basin, the Sycamore and overlying late Mississippian shales are roughly 500 to 2000 m thick (Johnson, 2008). Mississippian strata thin from about 1000 m in the western Anadarko Basin to about 100 m in the Cherokee Platform (Johnson, 2008). For almost all of Mississippian time, Kansas was a continental shelf environment, and received thick deposits of shallow marine carbonates (Zeller et al., 1968). The Pennsylvanian in Oklahoma was strongly influenced by orogenic activity, both locally and from the formation of the Ancestral Rocky Mountains in association with the Ouachita-Marathon orogeny (Johnson, 2008). Pennsylvanian tectonics are largely responsible for producing the region's present structural configuration, with southern and eastern mountainous areas juxtaposed with deep basins in Oklahoma's center that

grade into the shelf environments of northern Oklahoma and Kansas (Zeller et al., 1968; Johnson, 2008). A major unconformity exists between Pennsylvanian and Mississippian strata in both Oklahoma and Kansas (Zeller et al., 1968; Johnson, 2008). Pennsylvanian strata in Oklahoma are predominantly marine shale interbedded with sandstones and carbonates and vary in thickness from < 1500 m in the northern shelf areas up to 5500 m in Oklahoma's central and southern basins (Johnson, 2008). Historically, these strata have been the most important producers of oil and gas in the state (Johnson, 2008). In Kansas, the Pennsylvanian is recorded in cyclic deposits of marine shales and limestones separated by nonmarine deposits (Zeller et al., 1968). These cyclic deposits grade into the thicker shales and sandstones of Oklahoma's basins (Zeller et al., 1968). The NFZ formed during Pennsylvanian time and imparts a slight, localized, eastward dip on Mississippian and Pennsylvanian strata (Zeller et al., 1968; Johnson, 2008).

In Early Permian time, a shallow sea flooded western Oklahoma, leaving marine limestones and shales in its center and "red beds" (red shales and sandstones) on its margins (Johnson, 2008). Subsequently, these seas largely evaporated leaving thick salt and gypsum/anhydrite deposits (Johnson, 2008). Much of the relief of Oklahoma's southern and eastern highlands was removed by erosion by the Late Permian (Johnson, 2008). Permian strata in Oklahoma range in thickness from 300-1500 m (Johnson, 2008). Similarly, Permian deposits in Kansas are characterized by limestones grading upwards into red siltstones and shales and finally into thick evaporite deposits (Zeller et al., 1968). Much of Oklahoma's modern surficial geology is dominated by Permian sediments, particularly in central and western Oklahoma (Johnson, 2008). East of the Nemaha uplift, Pennsylvanian bedrock is juxtaposed with the Mississippian-Pennsylvanian uplifts of the Ozark Dome and the Ouachita and Arbuckle mountains (Johnson, 2008).

Throughout the Early to Middle Mesozoic, most of Oklahoma was probably above sea level (Johnson, 2008). With the exception of isolated fluvial and lacustrine deposits in central Oklahoma, sediments from this time period only exist today in the state's Panhandle (Johnson, 2008). In contrast, Cretaceous shallow seas covered much of Oklahoma, where the eastern and northeastern reaches were probably above sea level at this time while the southeast was inundated by the Gulf of Mexico (Johnson, 2008). Though extensively deposited, Cretaceous strata have largely been eroded after the Laramide Orogeny imparted a general eastward dip to Oklahoma's stratigraphy, which drained the recurring shallow seas from the state for the final time in its geologic history (Johnson, 2008). In Kansas, the Mesozoic is also dominantly represented by Cretaceous sediments, mostly in the form of shale though with significant deposits of the nonmarine Cheyenne and Dakota Sandstones (Zeller et al., 1968). These Cretaceous deposits persist in the western half of Kansas today (Zeller et al., 1968). Tertiary time saw deposition of alluvial and eolian sediments from the Rocky Mountains (Zeller et al., 1968; Johnson, 2008). The Ogallala formation, which is the primary groundwater-producing unit in the High Plains Aquifer System (Ryder, 1996) is present only in the western parts of Oklahoma and Kansas at thicknesses of ~70-200 m (Jones, 2008; Zeller et al., 1968). Additional alluvial sediments were deposited as glaciation advanced over the northern US during the Quaternary (Johnson, 2008; Zeller et al., 1968). Modern topography, soils, and drainage systems were shaped by Pleistocene erosional processes (Johnson, 2008; Zeller et al., 1968).

The most prominent geologic structure throughout the study area is the Nemaha Fault Zone (NFZ), which is a major north-south trending fault zone extending from eastern Nebraska through eastern Kansas and into central Oklahoma. Interpreted as a deeply penetrating Pennsylvanian structure of compressional origin later reactivated in strike-slip motion, the NFZ terminates at the

shear zone demarcating the northern extent of Oklahoma's southern highlands (Gay, 2003; McBee, 2003). Its width ranges from ~24 km in northern Kansas to < 10 km in central Oklahoma (Gay, 2003; McBee, 2003). The main N-S trend of the NFZ does not place it at high risk for failure according to the roughly E-W direction of maximum regional tectonic stress measured by Alt & Zoback (2017) (Fig. 1). However, faults of various orientation are likely ubiquitous in intraplate settings (Townend & Zoback, 2000), which has been shown to be true in both Oklahoma (Marsh & Holland, 2016) and Kansas (Baar, 2015). Many of these faults are at optimal orientation for failure according the regional stress regime, and in fact known faults have been cited as the origins of major injection-induced earthquakes in Oklahoma (Alt & Zoback, 2017).

Hydrogeology & Hydrostratigraphy

Groundwater withdrawals for beneficial use in Oklahoma and Kansas are chiefly from three principal aquifer systems. The High Plains Aquifer System is developed in the western portion of the region, and the Western Interior Plains and Ozark Plateau Aquifer Systems are developed in the central and eastern areas (Jorgensen et al., 1997; Osborn et al., 2013). The Western Interior Plains and Ozark Plateaus systems consist of stratigraphically equivalent units but are considered separate groundwater flow systems (Osborn et al., 2013). The uppermost aquifer system in the study area is the Western Interior Plains system, which generally thickens from the shelf environments in the north to the deep basin environments in the south and dips to the south and west away from the Missouri River and the Ozark Plateau region, respectively (Osborn et al, 2013). The Western Interior Plains Aquifer System is confined from above by Pennsylvanian to Permian shales and evaporites (Jorgensen et al., 1997; Osborn et al., 2013). The aquifer system itself consists of interbedded limestones and sandstones that vary in thickness from 0 in northern Kansas to > 6000 m in the Anadarko Basin if deep, saline groundwater systems are

included (Osborn et al., 2013). The system is subdivided into an upper aquifer consisting of Mississippian limestones typically < 300 m in thickness and a lower aquifer of Cambrian to Devonian limestones, dolostones, and sandstones that are > 3000 m thick in the deep Anadarko Basin (Osborn et al., 2013). Laterally continuous Devonian shales hydraulically separate the upper and lower subdivisions of the Western Interior Plains Aquifer System (Jorgensen et al., 1997; Osborn et al., 2013) (Fig. 2). In most of the study area, TDS concentrations in both the upper and lower subdivisions of the Western Interior Plains Aquifer System are high enough to be considered brine (> 35,000 ppm) and are often an order of magnitude higher (Osborn et al., 2013; Ferguson et al., 2018). These fluids achieve such high TDS concentrations due to evaporite dissolution, long residence times (stagnation), minimal recharge, and low topographic gradients in the region (Osborn et al., 2013; Ferguson et al., 2018).

Of interest to this study are the Mississippi Lime hydrocarbon play, the late Cambrian to early Ordovician Arbuckle Group, Precambrian crystalline basement, and the Nemaha Fault Zone (NFZ). With the exception of thin, laterally discontinuous, early Cambrian sandstones, the Arbuckle Group directly and unconformably overlies Precambrian basement, and consists of Bonterre Dolomite, Eminence Dolomite, Gasconade Dolomite, the Roubidoux Formation, and Jefferson City/Cotter Dolomite (Franseen et al., 2004; Johnson, 2008) (Fig. 3). At the regional scale, the Arbuckle is hydraulically isolated from overlying units by late Ordovician to Devonian shales (Keranen et al., 2014; Suhm, 2016; Langenbruch et al., 2018; Rottmann, 2018.). The Mississippi Lime play has been the most important target for unconventional production over the last decade and produces a high cut of hypersaline brine (Mitchell & Simpson, 2015; Murray, 2015; 2016; Blondes et al., 2018). The Arbuckle is the primary target reservoir for injection disposal of this brine (Rottmann, 2018; Ansari et al., 2019). Arbuckle porosity is intercrystalline,

vuggy, karstic, and fractured (Franseen et al., 2003). A rough estimate of regional-scale Arbuckle porosity is 10% with an effective permeability of 5.0×10^{-13} m^2 (Morgan & Murray, 2015; Kroll et al., 2017). The Arbuckle is ideally suited for fluid waste disposal due to its regional underpressure relative to hydrostatic, which may be the result of paleokarst development (Mitchell & Simpson, 2015; Rottmann, 2018), porosity enhancement via dolomitization (Jones et al., 2005), and hydraulic connection to Precambrian basement through an extensive fracture network (Rottmann, 2018). The latter feature is likely what causes pore pressure transients to transmit from the Arbuckle to seismogenic depths (Langenbruch et al., 2018; Rottmann, 2018; Pollyea et al., 2019). Fault zones are known to exhibit complex hydrogeologic behavior, particularly in regard to permeability (Bense et al., 2013), which has been shown to have strong effects on fluid pressure propagation in relation to injection induced seismicity (Vadacca et al., 2018, Yehya et al., 2018). Depending on the geologic setting in which a fault occurs, the fault can serve as: 1) a barrier to fluid flow across the fault strike; 2) a conduit to fluid flow parallel to fault strike; or 3) a combined conduit/barrier to fluid flow (Bense et al., 2013). Figure 4 shows a schematic representation of a fault serving as a combined conduit/barrier. In this situation, the fault cuts through a matrix of unfractured rock, and the fault core consists of fine-grained fault gouge restricting cross-strike fluid flow. Enclosing the fault core is a damage zone containing a dense fracture network, which enhances fluid flow parallel to fault strike.

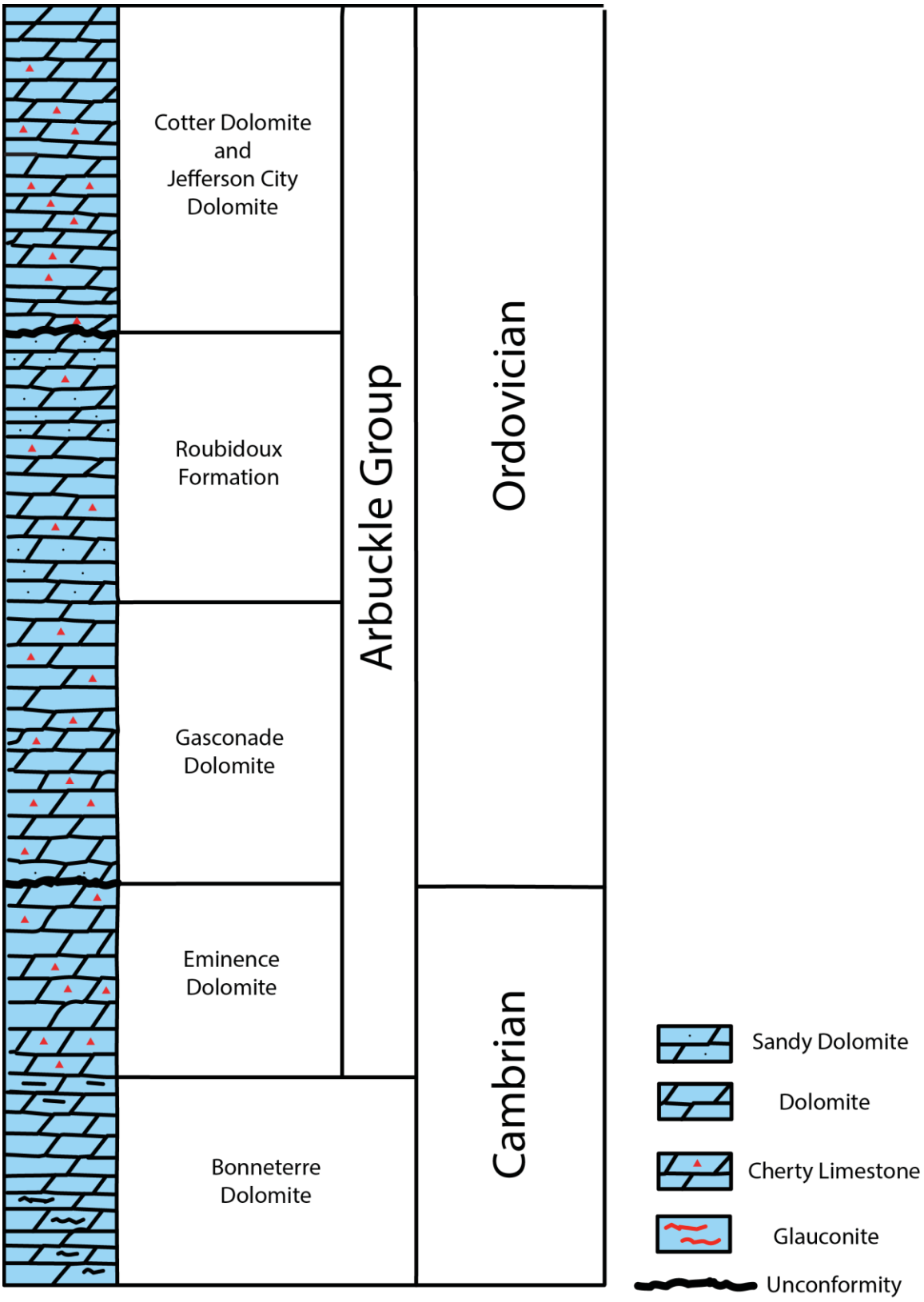

Figure 3: Arbuckle Group stratigraphic column modified from Franseen et al. (2004).

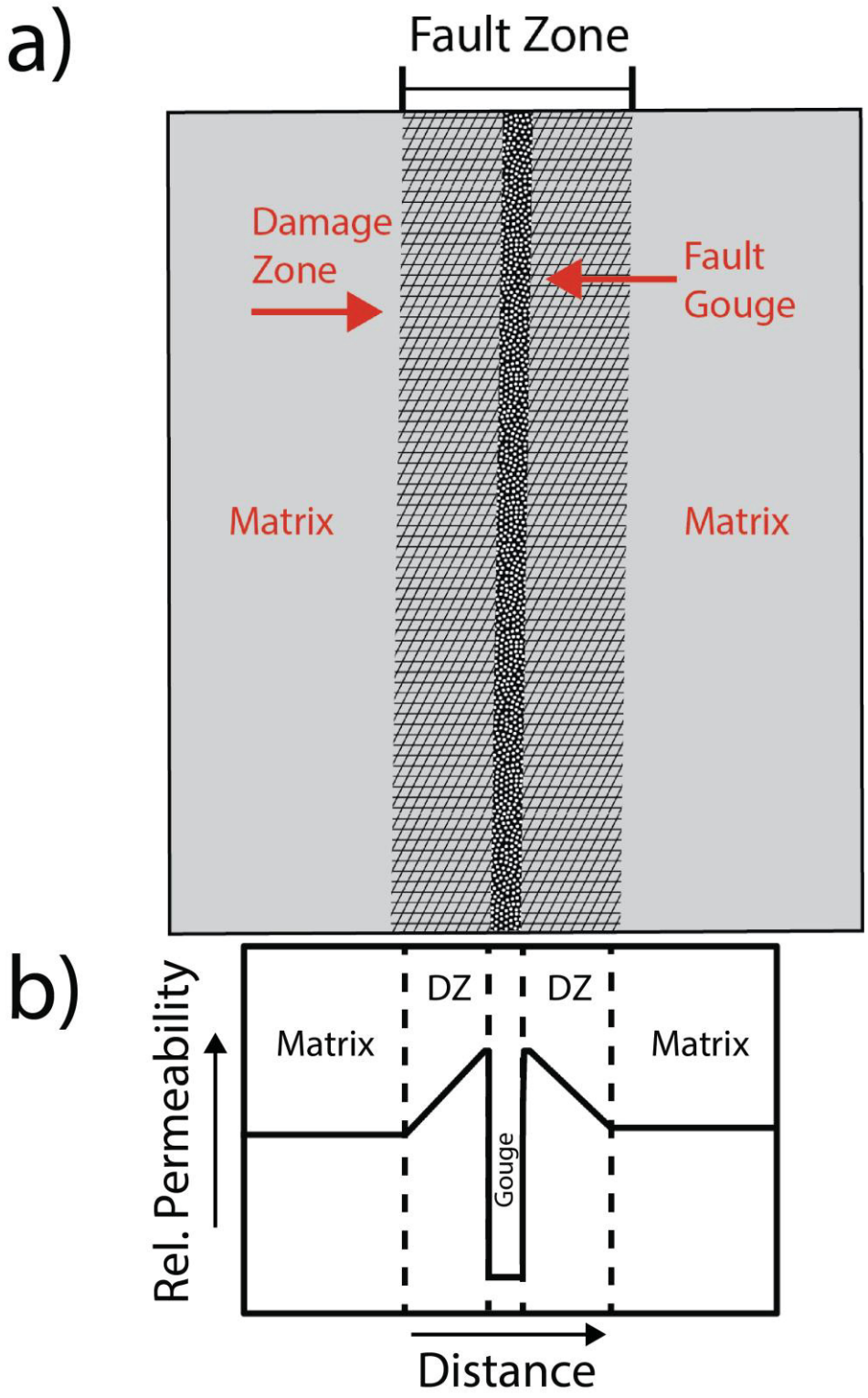

Figure 4: Schematic representation of combined conduit/barrier fault zone permeability. a) Fault cutting through unfractured rock matrix consists of fault core enclosed by damage zone. b) Relative permeability across the fault modified from McCallum et al. (2018).

METHODS

Geologic Model

This study is based on a regional-scale model of oilfield wastewater disposal across central Oklahoma and south-central Kansas. The conceptual model is based on regional-scale architecture of the Arbuckle Group and underlying Precambrian basement. In this conceptual model, the Arbuckle Group is hydraulically disconnected from overlying geologic formations by regionally extensive, low-permeability late Ordovician shales. As a consequence, the overlying geology is grouped into an 'overburden' subdomain and generally neglected for the model domain developed in this study. Structure contour data for the top of the Arbuckle and Precambrian basement are obtained from the Oklahoma Geological Survey (OGS) via internet download (Crain et al., 2018) and visualized using ArcMap™. Each dataset is transformed into a continuous raster with 10-km cell size using bilinear interpolation (Fig. 5). Upon rasterization, the original spatial datum is transformed from the Albers Equal Area Conic projected coordinate system to Universal Transverse Mercator Zone 14 N for consistency with the metric unit system, which is implemented in the numerical modeling software. Each raster is then converted into a shapefile with *xyz* points representing the center of each grid cell (*xy*) and elevation (*z*) corresponding to mean sea level (msl). The *xy*-coordinate pairs (easting, northing) are

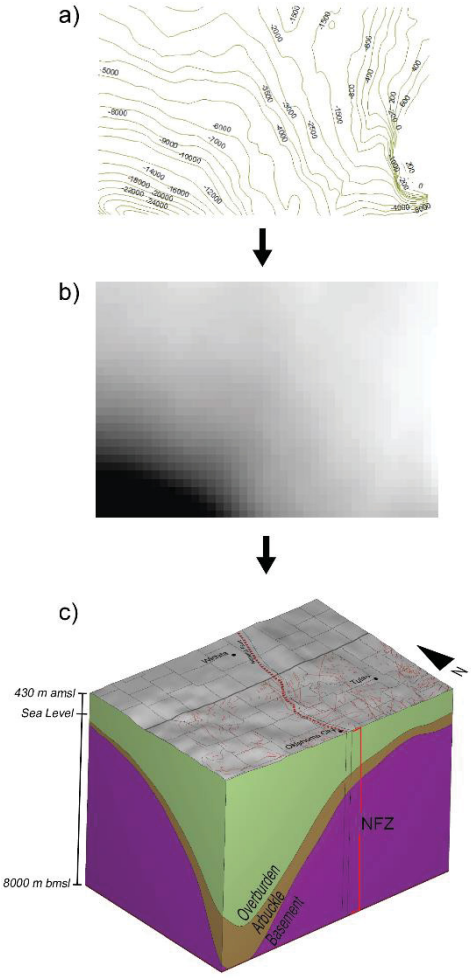

Figure 5: Generation of conceptual model geometry. Structure contour maps (a) are converted to surface rasters (b) via bilinear interpolation, which are then used to triangulate the 3D model geometry (c).

added to the point-grid attribute table for each structure contour surface, and these tables are exported as comma-delimited ASCII files for use with the numerical modeling software. These structure contour surfaces are imported into the PetraSim numerical simulation code for generating a digital conceptual model comprising three subdomains: Overburden, Arbuckle Group, and Precambrian basement (Fig. 5).

The Nemaha Fault Zone (NFZ) is incorporated into the model in a similar manner to the surface data. For its Oklahoma portion, line features representing the NFZ are extracted from the OGS Interpretive Fault Database (Marsh et al., 2016) while paying special attention to features that run through the center of the "Nemaha Uplift" (Gay, 2003; McBee, 2003) in Grant, Garfield, Kay, and Noble Counties, where the NFZ begins to significantly increase in width. The Kansas portion of the NFZ is digitized from a trace map after Gay (2003). After merging all extracted and digitized line features, points are generated along the merged line with 10-km separation. To prevent smoothing, extra points are added for the merged fault trace's end points and in places where the trace makes sharp turns. Linear interpolation appends elevation values from the Arbuckle top surface raster, and an *xyz*-coordinate table is created and exported to reproduce the geologic structure within the groundwater flow simulator. The NFZ is conceptualized to have 10 km width throughout the model after (Gay, 2003; McBee, 2003). This is accomplished by duplicating the *xyz*-coordinate table with *x*-coordinates of ± 5 km from their original values; however, the actual width is reduced to ≤ 6 km after grid discretization and manually post-processing the grid cell connections.

Discretization

The conceptual model is laterally discretized into an unstructured grid via Voronoi tessellation that results in an irregular mesh with refined cell size in the study area (Fig. 5). The

mesh comprises polygonal grid cell geometry in the horizontal plane, which reduces potential for numerical errors that are known to occur when radial flow is simulated using regular Cartesian grid cells. Within the study area, grid blocks are typically 2 – 6 km wide. To mitigate non-physical effects associated with boundary feedbacks, the study area is bounded laterally by a 100-km wide buffer zone comprising grid cells that progressively increase in width from 10 – 30 km with distance from the study area. The domain is vertically discretized into grid cells with uniform 48 m thickness. The complete model domain is an unstructured mesh that reproduces regional geologic structure comprising the Anadarko Shelf in the northwest, Cherokee Platform in the north and east, the Anadarko Basin in the southwest, and the north-south trending NFZ, the latter of which penetrates the entire thickness of the model (Fig. 6).

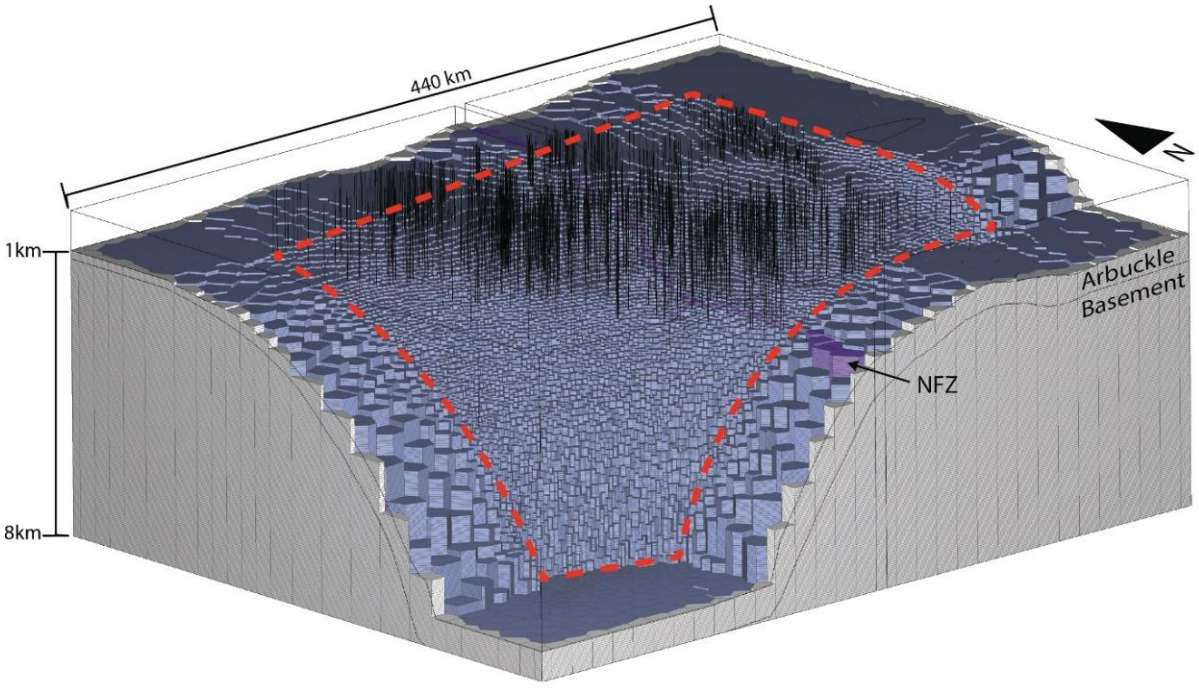

Figure 6: Discretized model domain with overburden removed. Blue represents the Arbuckle Group, purple the NFZ. The study area is outlined in red dashes; outside this area is a 100 km wide buffer zone. Vertical black lines show injection wells. The model comprises shelf environments in the north and east, the Anadarko Basin in the southwest, and the north-south trending NFZ, the latter of which penetrates the entire thickness of the model.

Injection Wells

The numerical model developed for this study includes all wastewater disposal wells that operate within or below the Arbuckle Group from 2006 to 2018. Well data are gathered from the Oklahoma Corporation Commission (OCC) and Kansas Geological Survey (KGS) (OCC Oil and Gas Data Files; Kansas Fluid Injection Database). Data for each well comprise its unique American Petroleum Institute (API) reference number, ground surface coordinates, depth, injection zone, and injection volume. Since well data are sourced from two different state organizations, two different pre-processing methodologies are employed. Oklahoma wells are first matched by API number. Custom shell scripts remove duplicates, format API numbers to 10-digits, and aggregate monthly injection volume data into yearly totals. These well records are formatted in ArcMap™ as shapefiles and clipped to the extent of the study area. The spatial reference datum for each record in the shapefile is converted from the native NAD 83 geographic coordinate system to the UTM zone 14 N projected coordinate system. After adding UTM coordinates and elevation data, these shapefiles are trimmed to those wells whose bottom depth is equal to or below the Arbuckle top surface. Pre-2011 OCC well data do not contain absolute well bottom depths, but instead packer depths. Wells in the pre-2011 data that match in location and/or API number to wells in the post-2011 data are joined to the latter dataset; otherwise, packer depths are assumed to be the injection interval and these data are processed as previously described. The 'joins and relates' function of ArcMap is employed to aggregate yearly well data into a single dataset comprising injections from 2006 – 2018.

Kansas well data are initially formatted in ArcMap™ in a similar fashion to the Oklahoma data, with the exception that Kansas data are originally spatially referenced to NAD 27 instead of NAD 83. The API number records for these data are largely nonunique, thus the data are joined

on UTM coordinates. To remove duplicate entries and aggregate injection volumes distributed across multiple entries for the same well and/or same year, the Kansas data are then manually edited according to the following methodology: (1) the complete 2006 – 2018 Kansas well dataset is exported from the GIS and opened in spreadsheet form; and (2) the data are systematically searched by sorting first on easting, then on northing. First, surface coordinates are compared; if two records are laterally separated by ≤ 10 m, they are considered to represent the same well. If separated by > 10 m but ≤ 100 m, the coordinates are verified with Google Maps™ satellite imagery; if only one well exists within a 100 m radius, the two records are judged to represent the same well. Between records identified as representing the same well, reported injection volumes are handled thus: (1) if volumes for the same year are identical, they are interpreted as duplicate entries, and only one is kept; or (2) if volumes for the same year differ, they are summed into one record. After all yearly well records are joined to one table per state, both state tables are merged into a master injection well database for the entire study area with a total 2,231 wells. To verify that no data is lost in processing, the master database is then related to the yearly tables, and record counts for each year are cross-checked. Wells are added to PetraSim via a custom shell script to format well data into an appropriate input table. The script ensures that individual injections occurring within the model domain are assigned as source terms to one grid block. The discretized model domain and injection well data are exported from PetraSim in a format that is compatible with the TOUGH3 numerical simulator.

Model Parameters

Effective permeability in the Arbuckle is specified as 5.0×10^{-13} m^2 (Morgan & Murray, 2015; Kroll et al., 2017), and generally assumed to be isotropic and homogeneous at the scale of the model developed for this study. Within the Precambrian basement, effective permeability is

modeled in accordance with the Manning & Ingebritsen (1999) equation for depth-decaying permeability (k),

$$k(z) = k_o(\frac{z}{z_o})^{-3.2} \quad (3)$$

where, z is depth, and k_o is permeability at the depth of the Arbuckle-Basement contact (z_o). Figure 7 shows depth-dependent permeability curves for two characteristic environments in the model: thin, platform and shelf environments and thick, deep basin environments. The NFZ is separated vertically into the portions that occur in the Arbuckle and basement. Because permeability characteristics of the NFZ are subject to substantial uncertainty, this study tests three fault permeability scenarios: a) impermeable (k_{xyz} = 0); b) isotropic, but very low permeability (k_{xyz} = 5.0 × 10^{-17} m^2) and c) anisotropic, where k is calculated according to Equation 3 with an anisotropy ratio of 1:10,000 (horizontal-to-vertical). Basement permeability structure is held constant for these three scenarios; in scenarios d) and e), k_o is raised and lowered by one order of magnitude, respectively, while the NFZ as held contant as impermeable as in a).

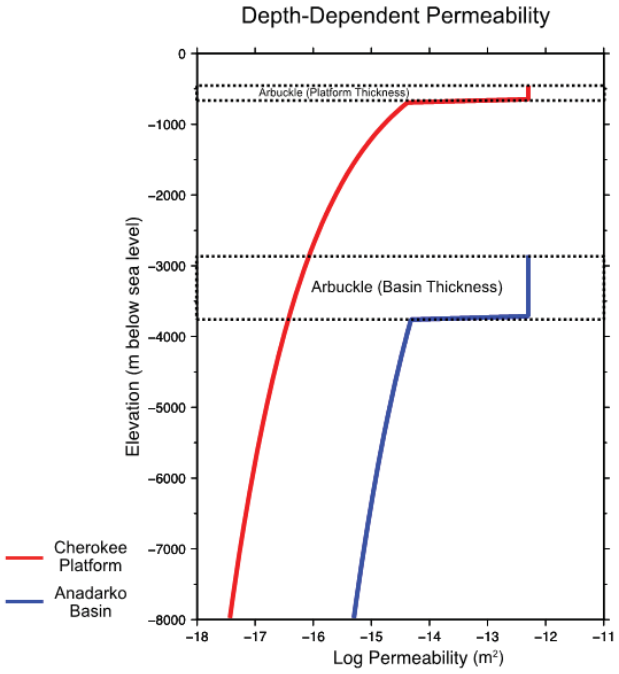

Figure 7: Depth-decaying basement permeability structure for platform/shelf (red) and deep basin (blue), the two main environments in the model domain.

Initial conditions are calculated on the basis of gravity and thermal equilibrium that assumes a constant, basal geothermal heat flux of 40 mW/m^2 (Cranganu et al., 1998), and atmospheric conditions comprising constant temperature and pressure of ~10 °C ~0.1 MPa. Fluid densities used in this model are derived from TDS concentrations taken from the USGS Produced

Waters Database (Blondes et al., 2017; Pollyea et al., 2019) (Table 1). TDS concentrations of brine samples from Precambrian Basement in Kansas with a typical value of 100,000 ppm are converted to a density of ~1063 kg/m^3 (at 52°C and 18 MPa). The resulting conditions represent a linear hydrostatic gradient with basal temperature and pressure of ~160°C and ~85 MPa. For injection simulations, Dirichlet conditions are imposed at the lateral boundaries to maintain the far-field pressure and temperature gradients and the overburden subdomain is removed, leaving the model top surface as a no-flow boundary representing a regional confining unit. Injected fluid is modeled with a density of 1117 kg/m^3 (at 52°C and 18 MPa), which represents 200,000 ppm TDS brine and is typical of oilfield brine produced from the Mississippian plays in northern Oklahoma and the Hunton dewatering play in eastern Oklahoma (Pollyea et al., 2019). Simulations are completed with the TOUGH3/EOS7 module (Appendix A) to account for the variable-density fluid flow (Jung et al., 2017). A full list of parameters is contained in Table 2.

Table 1: Composition of water produced from Mississippi Lime and Precambrian Basement in select counties of Oklahoma and Kansas

Region	State	Formation	Mean TDS (ppm)[a]	σ (ppm)	*N*	Density[b] (kg m^{-3})
Alfalfa Co.	OK	Miss. Lime	207,000	31,000	8	1123
Grant Co.	OK	Miss. Lime	235,000	30,000	54	1137
Barber Co.	KS	Miss. Lime	174,000	72,000	24	1106
Harper Co.	KS	Miss. Lime	201,000	35,000	2	1120
Sumner Co.	KS	Miss. Lime	215,000	43,000	11	1127
Central Kansas[c]	KS	Precambrian	107,000	43,000	10	1068

Data from USGS National Produced Waters Database (Blondes et al., 2018). σis one standard deviation. [a]Arithmetic mean. [b]Calculated at 40 °C and 21 MPa. [c]Data records from Rice, Rooks, Rush, Russel, and Barton Counties.

Table 2: Model Parameters

	k_h	*k*-Anisotropy	Porosity	Density	□	k_T	c_p	*D*
	m^2	h:v	-	kg m^{-3}	Pa^{-1}	W m^{-1} °C^{-1}	J kg^{-1} °C^{-1}	m^2 s^{-1}
Brine	-	-	-	1117†	-	-	-	1.14×10^{-9}
Arbuckle	5×10^{-13}	1:1	0.1	2,500	1.7×10^{-10}	2.2	1,000	-
NFZ (a)	0	1:1	0.1	-	-	2.2	1,000	-
NFZ (b)	5×10^{-17}	1:1	0.1	-	-	2.2	1,000	-
NFZ (c)	5×10^{-17}	1:10,000	0.1	-	-	2.2	1,000	-
Basement (k_o, abc)	5×10^{-15}	-	0.1	2,800	1.7×10^{-11}	2.2	1,000	-
Basement (k_o, d)	5×10^{-14}	-	0.1	2,800	1.7×10^{-11}	2.2	1,000	-
Basement (k_o, e)	5×10^{-16}	-	0.1	2,800	1.7×10^{-11}	2.2	1,000	-

†-Reference density for EOS7. All other densities represent values for rocks. Density and compressibility of NFZ is identical to surrounding layer (Arbuckle or Basement). *k*-permeability. β-compressibility. k_T-thermal conductivity. c_p-heat capacity. *D*-diffusion coefficient.

RESULTS

The groundwater model reproduces mean annual injection volume for 2,231 Underground Injection Control (UIC) wells operating between 2006 and 2018 in north-central Oklahoma and southern Kansas. The model continues through 2022 assuming annual 20% volume reductions for each well operating in 2018. The simulation is repeated for five unique permeability scenarios: the scenarios labeled a - c are permutations of permeability structure for the Nemaha Fault Zone (NFZ), while basement permeability is varied for scenarios d and e (Table 1).

Results are plotted as fluid pressure change with respect to initial conditions (hydrostat) for horizontal slices through the model domain at 5 km and 7 km depth below mean sea level (bmsl). Pressure change is presented as a polar color palette that ranges from red (overpressure) to white (hydrostat) to blue (underpressure). Earthquake hypocenter locations are superimposed on the pressure change maps for each year with symbols representing magnitude range; small gray circles represent M_w 2.5 - 3.9, larger maroon circles represent M_w 4.0 - 4.9, and green stars represent M_w 5.0 - 5.8. Figure 8 shows pressure change from hydrostat at 5 km bmsl, which is the typical hypocentral depth for included earthquakes in the study area, for model years 2011 and 2016. Although model data from 2006 - 2010 are not analyzed for this study, they are included in the simulation period because numerous studies show that this 'spin-up' is required to reproduce fluid pressure change leading up to the 2011 M_w 5.7 earthquake in Prague, Oklahoma (Keranen et al., 2014; Langenbruch et al., 2018; Zhai et al., 2020). Simulation data for 2016 is analyzed in regard to the three M_w 5+ earthquakes that occurred that year near Fairview, Pawnee, and Cushing, Oklahoma. During this study, real injection well data for Oklahoma and Kansas were complete through 2018. Results for the years 2019 – 2022 reflect annual 20% injection volume reductions from 2018 levels. These reductions test the effects of a gradual cessation of injection on pressure

propagation. Figure 9 shows pressure change at 7 km bmsl for model years 2011, 2016, and 2022, with wells active in 2011 and 2016 as well as basement surface contours overlaid. This depth is chosen to illustrate the effects of sinking, density-driven pressure transients, which will be discussed in the subsequent section. Figure 10 compares the results of this study and those of the Langenbruch et al. (2018) model, another regional-scale hydrogeological model of pressure change from fluid injection in Oklahoma and Kansas.

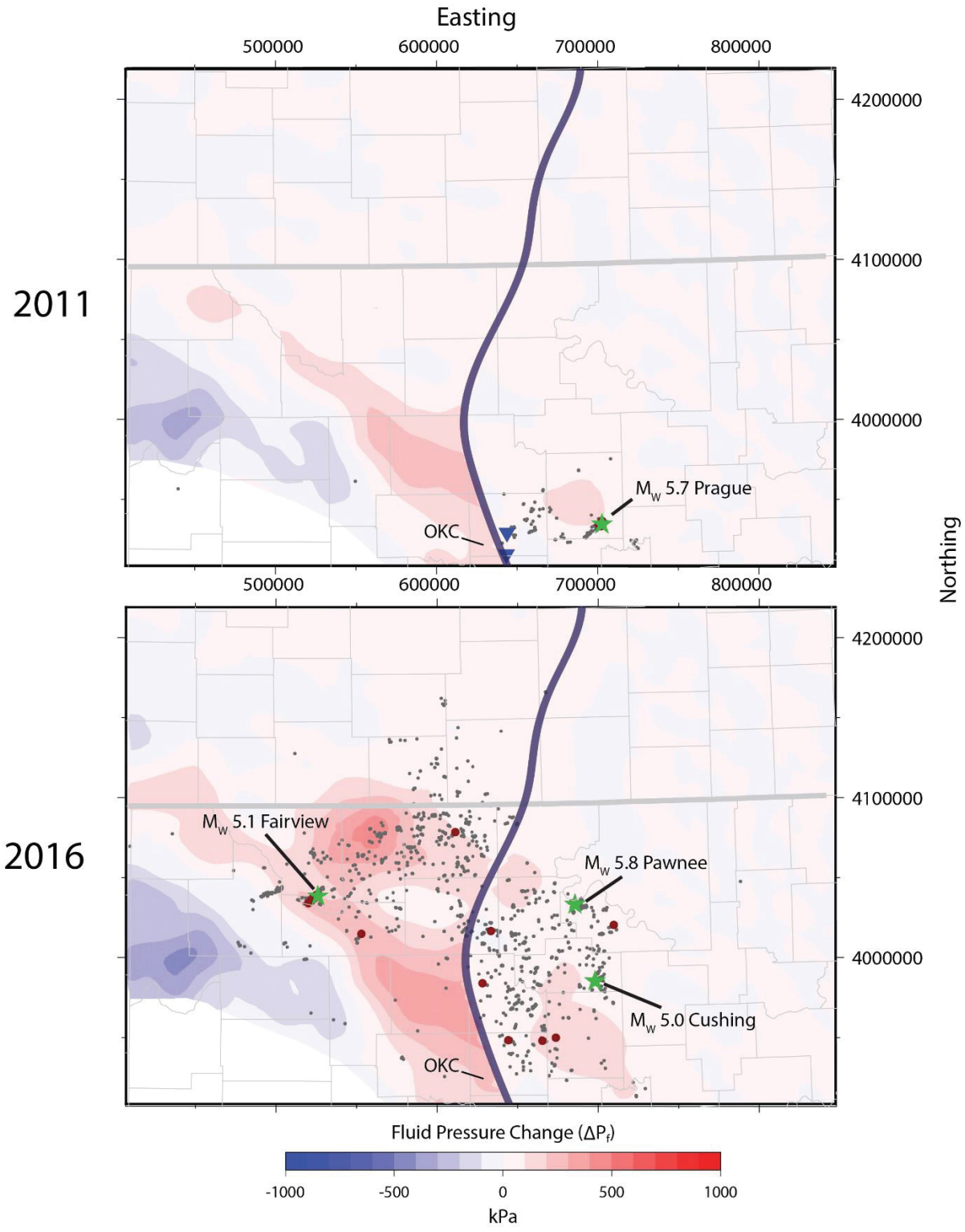

Figure 8: Modeled fluid pressure change relative to hydrostatic at 5 km bmsl for 2011 and 2016. Earthquakes for each year are plotted; gray circles = M_W 2.5 to 3.9, maroon circles = M_W 4.0 to 4.9, green stars = M_W 5.0 to 5.8. N-S trending blue curve is NFZ trace. OKC points to approximate location of Oklahoma City. Blue triangles in 2011 are southeast OKC high-rate injectors, shut in by 2016.

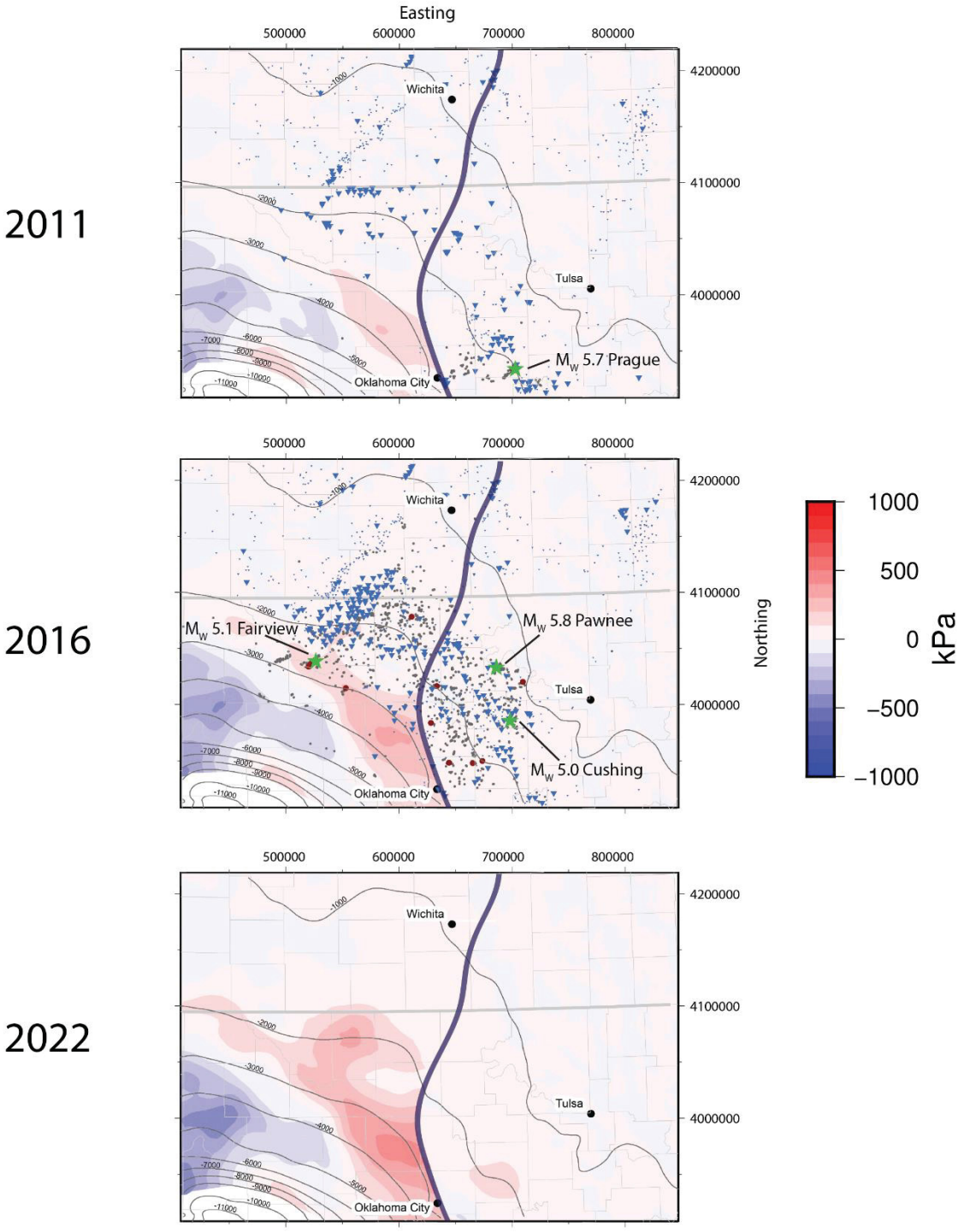

Figure 9: Fluid pressure change relative to hydrostatic for 2011, 2016, and 2022 at 7 km bmsl. Earthquakes and NFZ are plotted in the same manner as in Figure 8. Injection wells for 2011 and 2016 are graduated in symbol size according to injection volume. Note 100 kPa pressure front enveloping Mw 5.1 Fairview earthquake in 2016.

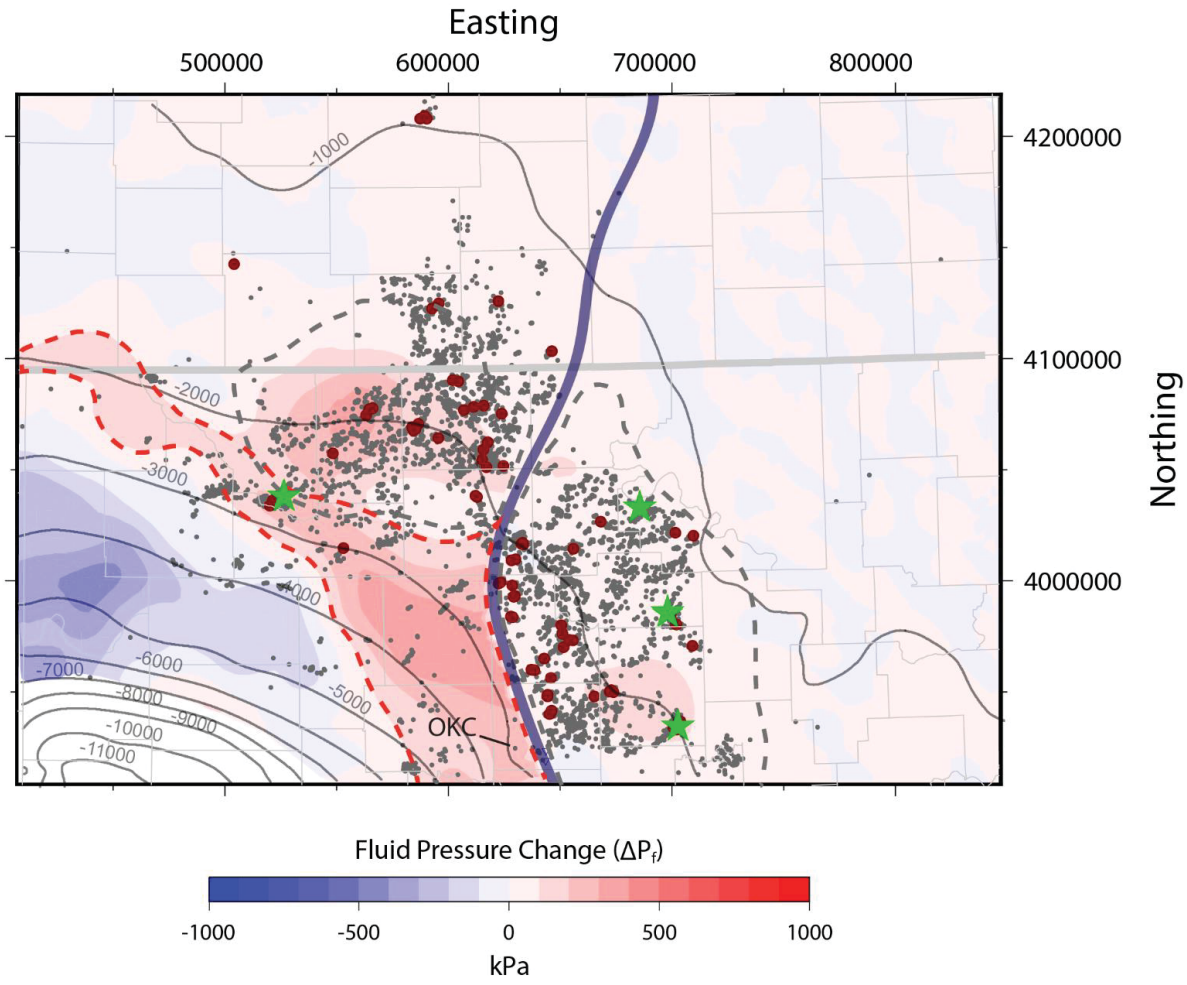

Figure 10: Simulated fluid pressure change relative to hydrostatic in December 2018 at 6 km bmsl (~6.5 km depth) for direct comparison to Langenbruch et al. (2018). Earthquakes and NFZ are plotted in the same manner as in Figures 8 and 9, but shown here are all earthquakes $M_W \geq 2.5$ for 2000 – 2018. Gray dashes outline the 100 kPa pressure front shown in the Langenbruch et al. (2018) hydrogeological model. Red dashes show density-driven pressure front responding to the steep dip of the Anadarko Basin.

DISCUSSION

The brittle crust is stressed to near its strength limit, so effective stress perturbations as low as ~10 kPa may be sufficient to induce failure on optimally oriented faults (Reasenberg & Simpson, 1992; Townend & Zoback, 2000; Ellsworth, 2013; Keranen et al., 2014). In Oklahoma and Kansas, the rapid increase in earthquake occurrence since 2009 indicates that critically stressed faults are pervasive throughout the region (Baar, 2015; Marsh & Holland, 2016; Alt & Zoback, 2017) (Fig. 1). Because wastewater injection decreases effective normal stress on critically stressed faults by increasing fluid pressure, numerical models of oilfield wastewater disposal are frequently implemented to show the relationship between earthquake sequences and injection-induced fluid pressure transients. In order to explain how fluid composition and map-scale structure affect spatial and temporal changes in fluid pressure transients, it is necessary to first discuss several of the seminal modeling studies that precede this work.

Numerical Models of Injection-Induced Seismicity

As injection-induced seismicity began propagating throughout the U.S. midcontinent, Zhang et al. (2013) developed a generic model of waste fluid injection into the Illinois Basin to investigate the mechanisms linking this injection to induced seismicity. The Zhang et al. (2013) model employs a hybrid analytical-numerical solution for a 2-D cross-section comprising a single-well injecting into a sedimentary reservoir containing linear fault zones (Zhang et al., 2013). Critical triggering stress along a fault plane is calculated from stress regime parameters in the US Midcontinent region (Zhang et al., 2013). These results show that injecting ~5500 m^3/day for 10 years may cause triggering fronts to propagate more than 4000 m deep into seismogenic basement when a vertical, high-permeability fault intersects the pressure front (Zhang et al., 2013). This study shows how fault zone hydraulics are highly effective at transmitting fluid pressure from

injection zones in the sedimentary strata to the seismogenic basement (Zhang et al., 2013). Interestingly, Zhang et al. (2013) mentions the importance that a density differential between injected fluid and native groundwater could have on the migration of pressure transients, but leave this as an open question.

Keranen et al. (2014) developed the first groundwater flow model of wastewater disposal in Oklahoma and found that the cumulative pressure effects that result from numerous, closely spaced injection wells were linked to the 2008 – 2012 Jones earthquake swarm. The model reproduces the Arbuckle Group as flat-lying and locally ~1000 m thick, which is juxtaposed above an 8 km thickness of underlying Precambrian basement (Keranen et al., 2014). Injections from 89 SWD wells are simulated from 1995 to 2012; these wells include four high-rate injectors in southeast Oklahoma City that collectively contribute ~640,000 m^3 per month (4,000,000 bbl/mo) (Keranen et al., 2014). This study also constrains an Arbuckle diffusivity of 2 m^2/s as the best fit to maximum wellhead pressures and local Arbuckle permeability measurements. Though all 89 modeled wells contribute to the overall fluid pressure disturbance, this study also shows that the 4 high-rate injectors are responsible for the majority of overpressuring, and thus they are assigned responsibility for triggering the 2008 – 2012 Jones earthquake swarm (Keranen et al., 2014). Keranen et al. (2014) illustrates the importance of 1) multiple injection wells in acting concurrently and in close proximity producing a combined, diffusional pressure front; and 2) the relationship between injection rates from individual wells and their contribution to the overall pressure disturbance. Also important is the observation that induced earthquakes do not occur until positive wellhead pressure is applied at injection wells (Keranen et al., 2014).

Langenbruch & Zoback (2016) developed a magnitude-exceedance prediction model linking SWD injection rates to induced seismicity. An analytical pressure diffusion model is used

to correlate pore pressure change to earthquake activity, but these pressure changes are not used in the corresponding probability-based risk assessment. Several M_w 4.7+ earthquakes that occurred in 2011 (Prague) and 2016 (Fairview, Cherokee, and Pawnee) are considered anomalous, and aftershocks for the 2016 large magnitude earthquakes are removed for model tractability. Furthermore, the Prague sequence is acknowledged as not fitting in the model at all, but that "a localized pressure increase in a limited area could always trigger seismicity on a given fault" (Langenbruch & Zoback, 2016). After injection decreases, as occurred in Oklahoma after government mandates and a drop in oil prices in 2015, fluid pressure decreases in the vicinity of wells while continuing to accumulate via diffusion in the far field; this implies that recovery (decrease) of seismicity to pre-injection rates will not be as quick as the increase in seismicity concurrent with injection (Langenbruch & Zoback, 2016). To enhance earthquake hazard predictions for Oklahoma, annual injection volumes above a determined triggering threshold are used to inform Poisson probability calculations (Langenbruch & Zoback, 2016). According to these methods, seismicity rates in Oklahoma are expected to return to pre-2009 levels within "a few years" (Langenbruch & Zoback, 2016). As with Keranen et al. (2014), this study neglects the effects of both fluid composition and regional-scale geologic structure.

Langenbruch et al. (2018) expands upon the model developed in Langenbruch & Zoback (2016) by including a physics-based, regional-scale numerical model of oilfield wastewater disposal. In this model, the effects of pore pressure diffusion and local variation in stress states are quantified via randomly distributed "seed points" representing randomly oriented faults. Injections from 809 wells operating in north-central Oklahoma and southeastern Kansas are simulated from 2000 to March 2018 (Langenbruch et al., 2018). The permeability structure in this model is isotropic with layered heterogeneity to account for the Arbuckle Group and Precambrian basement

(Langenbruch et al., 2018); however, this model also assumes horizontal layering, which neglects map-scale geologic structure. Injections occur at a uniform ~2 km depth into the Arbuckle Group reservoir, which is modeled with 4 km thickness and permeability ranging from 10^{-12} m^2 – 10^{-14} m^2 (Langenbruch et al., 2018). Precambrian basement is modeled with 17.5 km thickness and homogeneous and isotropic permeability ranging from 2×10^{-14} m^2 – 1×10^{-16} m^2. The NFZ is included as a nominally impermeable barrier to cross-strike fluid flow with a permeability of 10^{-20} m^2 (Langenbruch et al., 2018). Pressure diffusion from this 3-D numerical model is coupled with a finely discretized seismogenic index model to improve the magnitude-exceedance probability calculations established in Langenbruch & Zoback (2016). This study concludes that basement permeability (calibrated to 2×10^{-15} m^2) is the strongest control on the timing of propagation of fluid pressure transients to seismogenic depths. Furthermore, Langenbruch et al. (2018) finds that regional pressure increase is correlated with seismicity, while local-scale pressure changes are unrelated to earthquakes in the same locality. In other words, the cumulative effects of numerous, closely spaced injection wells drive far-field pressurization, which results in decreasing effective stress and induced-seismicity across central Oklahoma and southern Kansas (Langenbruch et al., 2018). According to their model, the pressurization rate (and thus earthquake rate) at 6.5 km depth returns to pre-2009 levels in 2020 (Langenbruch et al., 2018). In effect, injection rate reductions should reduce the occurrence of induced earthquakes (Langenbruch et al., 2018). While this study is useful in beginning to incorporate groundwater physics into probabilistic hazard prediction of induced seismicity, the model upon which these predictions are based also neglects geologic structure and fluid composition.

The aforementioned studies each assume that effective stress change is the only mechanism responsible for injection-induced earthquakes; however, several recent studies suggest that solid

elastic stress change may also cause earthquakes (Goebel et al., 2017; Norbeck & Rubinstein, 2018; Bhattacharya & Viesca, 2019; Zhai et al., 2020). Goebel et al. (2017) uses semi-analytical poroelastic stressing models to explain earthquakes occurring tens of km away from high-rate injection wells and beyond the extent of simulated pressure fronts. That study demonstrates that elastic stressing propagates through solid rock faster and to longer distances from injection wells than fluid pressure diffusion (Goebel et al., 2017). The study concludes that poroelastic stressing is responsible for triggering earthquakes at distances up to 50 km from injection wells (Goebel et al., 2017). Other studies that have compared the effects of pore pressure diffusion and solid elastic stress transfer on induced seismicity (Yeck et al., 2016; Bhattacharya & Viesca, 2019; Zhai et al., 2020) have generally agreed with this conclusion; however, it is important to note is that Goebel et al. (2017) also assumes flat-lying geology and constant fluid properties.

Fluid Composition & Injection-Induced Seismicity

Beginning in 2010, hydrocarbon production throughout Oklahoma and Kansas has been dominated by fracking in the Mississippi Lime play, which produces a high cut of hypersaline brine (Mitchell & Simpson, 2015). This fluid is characterized by ~200,000 ppm TDS concentration, which corresponds with a density of ~1120 kg/m^3 at 40 °C and 21 MPa (Blondes et al., 2018; Pollyea et al., 2019). Mississippi Lime brines are injected into the Arbuckle Group, which is in hydraulic connection with Precambrian basement where TDS concentrations are thought to be ~100,000 ppm with ~1068 kg/m^3 at the same pressure and temperature conditions (Blondes et al., 2018; Pollyea et al., 2019). Pollyea et al (2019) tested the implications of variable density fluid flow by modeling injections in the upper 200 m of a 400 m thick Arbuckle formation (characteristic of the Anadarko Shelf region) with a permeability of 5×10^{-13} m^2. Precambrian basement is modeled to a depth of 10 km (7700 m thickness) and is represented by a dual matrix-

fracture continuum amounting to a depth-decaying permeability of 1×10^{-14} m^2 – 9×10^{-17} m^2 (Pollyea et al., 2019). Both variable density and constant density models are simulated to 10 years of injection at a constant rate of 2080 m^3/day (13,000 bbl/day, characteristic of typical of high-rate injectors in the Anadarko Shelf region) followed by 40 years of recovery after injection is halted (Pollyea et al., 2019). Comparing the two models reveals the drastic effects that variable density has on the magnitude, size, and persistence of density-driven pressure transients (Pollyea et al., 2019). While the constant density model reaches a pressure disturbance of 10 kPa at 6 km depth after 10 years of injection, the variable density model pushes a 10 kPa pressure front to > 10 km depth and twice as far laterally after 10 years (Pollyea et al., 2019). Moreover, the constant density model recovers to a pre-injection pressure state almost immediately after injection stops, while the variable density model shows significant overpressure continuing to sink beyond the modeled time window. Additionally, overpressure at shallow depths collapses in response to the vanishing hydraulic gradient resulting from well shut in, while a high hydraulic gradient persists between the center of mass of the injected waste fluid and the ambient formation water (Pollyea et al., 2019). The rate at which the 10 kPa pressure front sinks is shown to temporally match the rate of hypocenter depth increase (Pollyea et al., 2019).

Map-Scale Structure, Fluid Composition & Injection-Induced Seismicity

Previous research shows that injection induced seismicity is explained by: 1) effective stress change driven by pressure diffusion, which is exacerbated by multiple injection wells according to the hydrogeologic principle of superposition (Keranen et al., 2014; Peterie et al., 2018; Langenbruch et al., 2019; Pollyea et al., 2020); 2) solid elastic stress transfer extending the reach of a diffusional triggering front (Goebel et al., 2017); and 3) advective, density-driven pressure transients causing effective stress change to occur deeper into seismogenic basement (Pollyea et

al., 2019). Numerical simulations presented in this thesis illuminate another fundamental control on the physical process of injection-induced seismicity: ***the interaction between variable density flows and significant regional stratigraphic dip***.

The similar regional setting between models in this study and those developed in Langenbruch et al. (2018) facilitates direct comparison. Both models show remarkable agreement in the magnitude and geometry of the regional pressure front on the east and west sides of the Nemaha Fault Zone (Fig. 10). This agreement is particularly apparent in the north Oklahoma pressure region centered on Alfalfa County (Fig. 10). In both models, this pressure front propagates north to align with triggered earthquakes in Harper and Sumner Counties, Kansas. Similar agreement in pressure front geometry can be seen between the two models in the Cherokee Platform geologic province to the east of the NFZ. At the local scale, this new model also compares favorably with Keranen et al. (2014), where the pressure front migrating east from Oklahoma City encompasses the Jones earthquake swarm (Fig 8). In this region, the geology is characterized by low structural gradients, so pressure diffusion is the first-order control on earthquake occurrence. Notably, the new model also places the 2011 M_w 5.7 Prague earthquake on the leading edge of a ~200 kPa pressure front radiating east from SE Oklahoma City. This result suggests that high-density wastewater may be driving longer-range pressure transients than previously considered for this region. Similar agreement between the models can be seen for the 2016 M_w 5.8 Pawnee and M_w 5.0 Cushing earthquakes.

Examining the southwestern portion of the study area, where the Anadarko Basin dips dramatically to the southwest, reveals the fundamental differences between the present study and regional-scale models by Langenbruch et al. (2018), Goebel et al. (2017), Zhai et al. (2020), and others. Each of these latter studies neglect both regional-scale structure (dipping strata) and

differences in fluid composition. Comparing the fluid pressure fronts simulated in these previous models with the current study shows that the combination of map-scale structure and high-density wastewater causes a broad region of overpressure to develop along the margin of the Anadarko Basin. This is apparent in Figures 8—10 as a NW-SE trending region of overpressure that stretches northwest from central Oklahoma to the northwestern border with Kansas.

This phenomenon can be explained by recent research demonstrating that high-density wastewater tends to sink (Pollyea et al., 2019), which suggests that density-driven pressure transients may cause advective flow to migrate down structural dips as buoyancy forces exceed equivalent freshwater head gradients (Bachu, 1995; Ferguson et al., 2018). In Oklahoma, the Anadarko Basin dips strongly to the southwest, and the present model suggests that high-density wastewater injected in north-central Oklahoma (Pollyea et al., 2019) may be following this structural depression downdip. Interestingly, this region has experienced a number of M_w 3+ earthquakes that fall outside the overpressure region presented by Langenbruch et al. (2018). The inability of Langenbruch et al. (2018) to match fluid pressure transients with these earthquakes (Fig. 10) is likely a result of oversimplifying the regional geologic structure and neglecting fluid composition. Specifically, the homogeneous and isotropic basement permeability used in Lagenbruch et al. (2018) allows pressure transients to dissipate too quickly relative to the more widely accepted depth-decaying permeability structure of Precambrian basement (Manning & Ingebritsen, 1999). Furthermore, the universally flat-lying hydrostratigraphy in the Langenbruch et al. (2018) model misses the significant regional dip into the Anadarko Basin in the southwestern part of the study area (Crain & Chang, 2018). As a result, the Langenbruch et al. (2018) model cannot capture the effects of buoyancy forces acting against freshwater head gradients where the regional dip is sufficiently high (Bachu, 1995; Ferguson et al., 2018).

Previous studies have demonstrated that fluids in deep sedimentary basins are characterized by high TDS concentrations (and thus high densities), particularly in the central and eastern United States (CEUS). These high-TDS brines occur in deep basins in part due to the down-dip flow of high-density brines against equivalent freshwater heads (Bachu, 1995; Ferguson et al., 2018). Injection of fluid waste of significantly higher density than preexisting formation water into a sedimentary basin with a sufficiently high structural gradient causes induced pressure transients to mirror this natural process, propagating down the regional dip to the southwest into the deeper parts of the basin.

The combined effects of map-scale structure and high-TDS brine disposal are perhaps most intriguing in the context of the 2016 M_w 5.1 earthquake in Fairview, Oklahoma. To examine the Fairview earthquake sequence, Goebel et al. (2017) uses a constant-density pressure diffusion model to show that fluid pressure from injection wells ~40 km away does not reach the site of the Fairview event, and instead shows that solid stress transfer is most likely responsible for inducing this earthquake. This latter result is generally supported by Langenbruch et al. (2018), which shows the Fairview earthquake outside the northern Oklahoma pressure region, where overpressure is < 0.1 MPa (Fig. 10). In contrast, the model developed here shows continuous fluid pressure transients forming a band around the border between the shelf and basin environments, with pressures in excess of 0.1 MPa enveloping the location of the Fairview earthquake (Fig. 10). This result suggests that regional-scale wastewater injection operations in northern and west-central Oklahoma may have generated sufficient fluid pressure to trigger the Fairview earthquake by effective stress change, rather than elastic stress transfer, as is now generally accepted. In addition to the Fairview earthquake sequence, no previous models explain the earthquakes occurring in the deeper parts of the Anadarko Basin to the southwest, which began to occur regularly by 2016.

These earthquakes are best explained by density flows being driven into the basin. With time, the high-magnitude pressure transients move away from high-rate injectors and down-dip into the deep basin.

As wastewater injection volume decreases throughout Oklahoma and Kansas, the earthquake rate is likely to fall (Langenbruch & Zoback, 2016, Zhai et al, 2020); however, this decreasing earthquake rate may be accompanied by a larger relative proportion of high-magnitude earthquakes (Pollyea et al., 2019). This phenomenon occurs because Pollyea et al. (2019) showed that the Gutenberg-Richter *b*-value decreases with depth in northern Oklahoma and southern Kansas. Moreover, continued propagation of fluid pressure transients into the deep Anadarko Basin may eventually interact with the Frontal Wichita fault system (FWFS), which is a NW-SE trending fault network that forms the boundary between the deepest part of the Anadarko Basin and the Wichita Uplift (Crone & Luza, 1990). Most of these faults originated in the Paleozoic, evidenced by the rocks they offset (Crone & Luza, 1990). Perhaps the most studied of these, the Meers Fault, shows evidence of Holocene seismic activity with magnitudes of up to 7 (Crone & Luza, 1990). This thesis does not conclude that such an event would be triggered by the density-driven pressure transients described above; only that a future interaction between pressure transients and the FWFS is possible. Moreover, if TDS concentrations continue to increase with depth in the Anadarko Basin, density-driven pressure transients could be arrested upon contact with regions of equal or greater fluid density. Further tectonic, structural, and hydrogeochemical analysis of the deep Anadarko Basin and FWFS is needed to sufficiently constrain the risk of injection-induced seismicity in this region.

In order to test the robustness of the model developed for this study, variations of the NFZ and basement permeability structures demonstrate that parametric variability influences the

magnitude and timing of pressure accumulation at a given point in the model (Apx B). However, when comparing these permeability permutations to the regional-scale patterns of overpressuring, geologic structure is shown to be the most important control on fluid pressure propagation when regional dip and density differences are sufficiently high. In the virtually flat-lying areas of the Anadarko Shelf and Cherokee Platform, pressure diffusion dominates. In the southwestern portion of the study area, our models consistently show pressure transients spreading along the margin of the Anadarko Basin and flowing down-dip where the regional structural grade exceeds 1%.

CONCLUSIONS

In the Anadarko Shelf of north-central Oklahoma and southeastern Kansas, a density differential between injected waste fluids and pre-existing formation brines implicates buoyancy force as a significant driver of regional groundwater flow. The modeling study presented in this thesis demonstrates that density-driven fluid flow drives fluid pressure transients down-dip into the deep Anadarko Basin. The discovery of down-dip density flows in the Anadarko Basin is important, because

- Down-dip density flows offer a new perspective on the causal mechanisms behind injection-induced seismicity.
- Earthquakes occurring in the deep Anadarko Basin cannot be explained by models that consider only pore pressure diffusion and/or solid elastic stressing.
- Significant variation in fluid composition is common in the sedimentary basins of the CEUS, where there is great potential for unconventional hydrocarbon production, and thus fluid waste disposal.
- Further propagation of pore pressure transients in the Anadarko Basin to the southwest may alter stress in the vicinity of the Meers Fault, on which geologic evidence implies Holocene earthquake activity of ~M_W 7.
- Regulation of fluid waste disposal can be informed by examinations of fluid composition and local geologic structure.

In addition to fluid composition and geologic structure, tectonics and local stress states on basement faults must be constrained in order to understand the seismic risk from geologic fluid waste disposal. This understanding is particularly important in regions similar to the deep Anadarko Basin and Wichita Uplift, where evidence indicates recent, major seismic activity.

Further research on stresses acting on faults in deep basin environments may illuminate how different fault regimes and orientations will respond to pore pressure elevated by high-density fluid waste injection.

REFERENCES

Ake, J., Mahrer, K., O'Connell, D., and Block, L., 2005. Deep-injection and closely monitored induced seismicity at Paradox Valley, Colorado. Bulletin of the Seismological Society of America, v. 95, no. 2, p. 664-683.

Alt, R. C. III, and Zoback, M. D., 2017. In situ stress and active faulting in Oklahoma. Bulletin of the Seismological Society of America, v. 107, p. 216-228.

Ansari, E., Bidgoli, T. S., and Hollenbach, A., 2019. Accelerated fill-up of the Arbuckle Group and links to U.S. midcontinent seismicity. Journal of Geophysical Research: Solid Earth, v. 124, p. 2670-2683.

Baars, D. L., 2015. Basement tectonic configuration in Kansas. Kansas Geological Survey Bulletin 237.

Bachu, S., 1995. Flow of variable-density formation water in deep sloping aquifers: review of methods of representation with case studies. Journal of Hydrology, v. 164, p. 19-38.

Bense, V. F., Gleeson, T., Loveless, S. E., Bour, O., and Scibek, J., 2013. Fault zone hydrogeology. Earth-Sciences Review, v. 127, p. 171-192.

Bhattacharya, P., and Viesca, R. C., 2019. Fluid-induced aseismic fault slip outpaces pore-fluid migration. Science, vol. 364, p. 464-468.

Blondes, M.S., Gans, K.D., Engle, M.A., Kharaka, Y.K., Reidy, M.E., Saraswathula, V., Thordsen, J.J., Rowan, E.L., and Morrissey, E.A., 2018, U.S. Geological Survey National Produced Waters Geochemical Database (ver. 2.3, January 2018): U.S. Geological Survey data release, https://doi.org/10.5066/F7J964W8.

Crain K. D., Chang, J. C., 2018. Elevation and thickness of the Ordovician Arbuckle Group in Oklahoma and surrounding states. Oklahoma Geological Survey Open-File Report OF2-2018.

Cranganu, C., Lee, Youngming, and Deming, D., 1998. Heat flow in Oklahoma and the south central United States. Journal of Geophysical Research: Solid Earth, v. 103, p. 27,101-27, 121.

Crone, A. J. and Luza, K. V., 1990. Style and timing of Holocene surface faulting on the Meers fault, southwestern Oklahoma. Geological Society of America Bulletin, v. 102, p. 1-17.

Downing, R. A., Edmunds, W. M., and Gale, I. N., 1987. Regional groundwater flow in sedimentary bains in the U.K. From Goff, J. C. & Williams, B. P. J. (eds). 1987, Fluid Flow in Sedimentary Basins and Aquifers, Geological Society and Special Publication No. 34, p. 105-25.

Ellsworth, W., 2013. Injection-induced earthquakes, Science, v. 341, p. 1-7.

Ferguson, G., McIntosh, J. C., Grasby, S. E., Hendry, J. M., Jasechko, S., Lindsay, M. B. J., and Luijendijk, E., 2018. The persistence of brines in sedimentary basins. Geophysical Research Letters, vol. 45, p. 4851-4858.

Franseen, Evan K., Byrnes, Alan P., Cansler, Jason R., Steinhauff, D. Mark, Carr, Timothy R., and Dubois, Martin K. (2003). Geological controls on variable character of Arbuckle reservoirs in Kansas: an emerging picture. Kansas Geological Survey Open-file Report 2003-59.

Franseen, E. K., Byrnes, A. P., Cansler, J. R., Steinhauff, D. M., and Carr, T. R., 2004, The geology of Kansas, Arbuckle Group. Current Research in Earth Sciences, bulletin 250, part 2.

Garrity, C. P., and Soller, D. R., 2009. Database of the geologic map of North America: adapted from the map by J. C. Reed, Jr. and others (2005). United States Geological Survey Data Series 424 [https://pubs.usgs.gov/ds/424/].

Gay, S. P. Jr., 2003. The Nemaha trend – a system of compressional thrust-fold, strike-slip structural features in Kansas and Oklahoma, parts 1 and 2. Shale Shaker, Jul-Aug 2003, p. 9-17; Sep-Oct 2003, p. 39-49.

Gay, S. P. Jr., 2014. Some observations on the Amarillo/Wichita Mountains thrust-fold belt and its extensions southeast into east Texas and northwest into New Mexico. Shale Shaker, Sept-Oct 2014, p. 338-366.

Goebel, T. H. W., Weingarten, M., Chen, X., Haffener, J., and Brodsky, E. E., 2017. The 2016 Mw 5.1 Fairview, Oklahoma earthquakes: evidence for long-range poroelastic triggering at >40 km from fluid disposal wells. Earth and Planetary Science Letters, vol. 472, p. 50-61.

Gugliemi, Y., Cappa, F., Avouac, J. P., Henry, P., and Ellsworth, D., 2015. Seismicity triggered by fluid-injection induced aseismic slip. Science, v. 348, p. 1224-1226.

Hadley, D. R., Abrams, D. B., and Roadcap, G. S., 2019. Modeling a large-scale historic aquifer test: insight into the hydrogeology of a regional fault zone.

Healy, J. H., Rubey, W. W., Griggs, D. T., and Raleigh, C. B., 1968. The Denver Earthquakes. Science, v. 161, no. 3848, p. 1301-1310.

Higley, D. K., Cook, T. A., and Pawlewicz, M. J., 2014. Petroleum systems and assessment of undiscovered oil an and gas in the Anadarko Basin province, Colorado, Kansas, Oklahoma, and Texas – Woodford Shale assessment units. Chapter 6 in Higley et al. 2014, Petroleum systems and assessment of undiscovered oil and gas in the Anadarko Basin province, Colorado, Kansas, Oklahoma, and Texas – USHS Province 58: US Geological Survey Digital Data Series DDS-69-EE, 24 p.

Holland, A., 2013. Earthquakes triggered by hydraulic fracturing in south-central Oklahoma. Bulletin of the Seismological Society of America, v. 103, no. 3, p. 1784-1792, doi: 10.1785/0120120109.

Horton, S., 2012. Disposal of hydrofracking waste fluid by injection into subsurface aquifers triggers earthquake swarm in central Arkansas with potential for damaging earthquake. Seismological Research Letters, v. 83, no. 2, p. 250-260.

Hsieh, P. A. and Bredehoeft, J. D., 1981. A reservoir analysis of the Denver earthquakes: a case of induced seismicity. Journal of Geophysical Research, vol. 86, no. B2, p. 903-920.

Johnson, Kenneth S. (2008). "Geologic History of Oklahoma." Oklahoma Geological Survey, Educational Publication 9: 2008.

Johnson, Kenneth S. (1989). "Geologic Evolution of the Anadarko Basin." Oklahoma Geological Survey Circular 90, 1989.

Jones, G.D., and Xiao, Y., 2005, Dolomitization, anhydrite cementation and porosity evolution in a reflux system: insights from reactive transport models. American Association of Petroleum Geologists, Bulletin, v. 89, p. 577–601

Jorgensen, Donald G., Helgesen, John O., Signor, Donald C., Leonard, Robert B., Imes, Jeffrey L., and Christenson, Scott C. (1997). "Analysis of Regional Aquifers in the Central Midwest of the United States in Kansas, Nebraska, and Parts of Arkansas, Colorado, Missouri, New Mexico, Oklahoma, South Dakota, Texas, and Wyoming—Summary." U.S. Geological Survey Professional Paper 1414 – A.

Ferguson, G., McIntosh, J. C., Grasby, S. E., Hendry, M. J., Jasechko, S., Lindsay, M. B. J., and Luijendijk, E., 2018. The persistence of brines in sedimentary basins. Geophysical Research Letters, v. 45, p. 4851-4858.

Frolich, C.m Hayward, C., Stump, B., and Potter, E., 2011. The Dallas-Fort Worth earthquake sequence: October 2008 through May 2009. Bulletin of the Seismological Society of America, v. 101, no 1., p. 327-340.

Jung, Y., Pau, G. S. H., Finsterle, S. and Pollyea, R. M., 2017. TOUGH3: A new efficient version of the TOUGH suite of multiphase flow and transport simulators. Computers & Geosciences, v. 108, p. 2-7.

Kansas Fluid Injection Database, accessed via http://www.kgs.ku.edu/Magellan/Qualified/fluid.html on October 20, 2019.

Keranen, K. M., Savage, H. M., Abers, G. A., and Cochran, E. S., 2013. Potentially induced earthquakes in Oklahoma, USA: links between wastewater injection and the 2011 M_w 5.7 earthquake sequence. Geology, v. 41, no. 6, p. 699-702, doi: 10.1130/G34045.1

Keranen, K. M., Weingarten, M., Abers, G. A., Bekins, B. A., and Ge., S., 2014. Sharp increase in central Oklahoma seismicity since 2008 induced by massive wastewater injection. Science, v. 245, i. 6195, p. 448-451.

Kim, W-Y., 2013. Induced seismicity associated with fluid injection into a deep well in Youngstown, Ohio. Journal of Geophysical Research: Solid Earth, v. 118, p. 1506-3518.

Kroll, Kayla A., Cochran, Elizabeth S., and Murray, Kyle E. (2017). Poroelastic properties of the Arbuckle Group in Oklahoma derived from well fluid level response to the 3 September 2016 M_w 5.8 Pawnee and 7 November 2016 M_w 5.0 Cushing earthquakes. Seismological Research Letters, v. 88 no. 4, pp. 963-970.

Langenbruch, C. and Zoback, M. D., 2016. How will induced seismicity in Oklahoma respond to decreased saltwater injection rates? Science Advances, v. 2, no. 11, p. 1-9.

Langenbruch, C., Weingarten, M., and Zoback, M. D., 2018. Physics-based forecasting of man-made earthquake hazards in Oklahoma and Kansas. Nature Communications, vol. 9, no. 3946, p. 1-10.

Manning, C. E., and Ingebritsen, S. E., 1999. Permeability of the continental crust: implications of geothermal data and metamorphic systems. Reviews of Geophysics, vol. 37, p. 127-150.

Marsh, S. and Holland, A., 2016. Comprehensive fault database and interpretive fault map of Oklahoma. Oklahoma Geological Survey Open-File Report OF2-2016.

McBee, W. Jr., 2003. Nemaha strike-slip fault zone. American Association of Petroleum Geologists Search and Discovery Article #10055.

McCallum, J., Simmons, C., Mallants, D., and Batelaan, O., 2018. Simulating the groundwater flow dynamics of fault zones. MODFLOW un-structured grid: a comparison of methods for representing fault properties and a regional implementation. Report by Australia Department of the Environment and Energy, National Centre for Groundwater Research and Training.

McNamara, D. E., Benz, H. M., Hermann, R. B., Bergman, E. A., Earle, P., Holland, A., Baldwin, R., and Gassner, A., 2015. Earthquake hypocenters and focal mechanisms in central Oklahoma reveal a complex system of reactivated subsurface strike-slip faulting. Geophysical Research Letters, v. 42, p. 2742-2749.

Mitchell, B. T., and Simpson, K., 2015. A regional re-evaluation of the Mississippi Lime play, south-central Kansas: the risks and rewards of understanding complex geology in a resource play. Paper prepared for presentation at the Unconventional Resources Technology Conference, San Antonio, Texas, USA 20-22 July 2015.

Morgan, Chance B. and Murray, Kyle E. (2015). “Characterizing Small-Scale Permeability of the Arbuckle Group, Oklahoma.” Oklahoma Geological Survey, Open-File Report (OF2-2015).

Murray, K. E., 2015. Class II saltwater disposal for 2009-2014 at the annual-, state-, and county-scales by geologic zones of completion, Oklahoma. Oklahoma Geological Survey Open-File Report OF5-2015.

Murray, K. E., 2016. Relationships between geologic zones, produced water, management, and seismicity in Oklahoma. American Association of Petroleum Geologists Search and Discovery Article #80519.

Narasimhan, T. N., and Witherspoon, P. A., 1976. An integrated finite difference method for analyzing fluid flow in porous media. Water Resources Research, vol. 12, p. 57-64.

Norbeck, J.H. and Rubinstein, J.L. (2018). "Hydromechanical Earthquake Nucleation Model Forecasts Onset, Peak, and Falling Rates of Induced Seismicity in Oklahoma and Kansas." *Geophysical Research Letters, 45,* 2963-2975.

Northcutt, R.A., and Campbell, J.A. (1996). "Geologic Provinces of Oklahoma." *Shale Shaker*; March-April 1996.

Oklahoma Corporation Commission, Division of Oil and Gas, UIC Injection Volumes 2006-2018. accessed via http://www.occeweb.com/OG/ogdatafiles2.htm on October 20, 2019.

Osborn, N. I., Smith, J. S., and Seger, C. H., 2013. Hydrogeology, Distribution, and Volume of Saline Groundwater in the Southern Midcontinent of the United States. United States Groundwater Resources Program, Scientific Investigations Report 2013-5017.

Peterie, S. L., Miller, R. D., Intfen, J. W., and Gonzales, J. B., 2018. Earthquakes in Kansas induced by extremely far-field pressure diffusion. Geophysical Research Letters, v. 45, p. 1395-1401.

Pollyea, R. M., Mohammadi, N., Taylor, J. E., and Chapman, M. C., 2018. Geospatial analysis of Oklahoma (USA) earthquakes 2011-2016: quantifying the limits of regional-scale earthquake mitigation measures. Geology, v. 46, no. 3, p. 215-218.

Pollyea, R. M., Chapman, M. C., Jayne, R. S., and Hao, W., 2019. High density oilfield wastewater disposal causes deeper, stronger, and more persistent earthquakes. Nature Communications, vol. 10, no. 3077, p. 1-10.

Pollyea, R. M., 2020. Explaining long-range fluid pressure transients caused by oilfield wastewater disposal using the hydrogeologic principle of superposition. Hydrogeology Journal, vol. 28, no. 2, p. 795-803.

Raleigh, C. B., Healy, J. H., and Bredehoeft, J. D., 1976. An experiment in earthquake control at Rangely, Colorado. Science, v. 191, p. 1230-1237.

Reasenberg, P. A., and Simpson, R. W., 1992. Response of regional seismicity to the static stress change produced by the Loma Prieta earthquake. Science, v. 255, no. 5052, p. 1687-1690.

Rottmann, Kurt (2018). "Well-Log Characterization of the Arbuckle Group in Central and Northern Oklahoma: Interpretation of the Impact of its Depositional and Post-Depositional History on Injection Induced Seismicity." Oklahoma Geological Survey Open-File Report 21-2018.

Ryder, P. D., 1996. Ground Water Atlas of the United States, Oklahoma, and Texas. United States Geological Survey GA 730-E.

Suhm, R. W., 2016. The Simpson play (including parts of the Arbuckle and Viola): stratigraphy and petroleum potential of Simpson Group (Ordovician), Oklahoma. Oklahoma Geological Survey Open File Report 3-2016.

Tóth, J., 1963. A theoretical analysis of groundwater flow in small drainage basins. Journal of Geophysical Research, vol. 68, no. 16, p. 4795-4812.

Townend, J. and Zoback, M. D., 2000. How faulting keeps the crust strong. Geology, v. 28, no. 5, p. 399-402.

United States Geological Survey 2020, ANSS Comprehensive Earthquake Catalog (ComCat). accessed via https://earthquake.usgs.gov/data/comcat/

Vadacca, L., Colciago, C. M., Micheletti, S., and Scotti, A., 2018. Effects of the anisotropy of the fault zone permeability on the timing of triggered earthquakes: insights from 3D-coupled fluid flow and geomechanical deformation modeling. Pure and Applied Geophysics, v. 175, p. 4131-4144.

Walsh III, F. R., and Zoback, M. D., 2015. Oklahoma's recent earthquakes and saltwater disposal. Science, v. 1, no. 5, p. 1-9.

Walter, J. I., P. Ogwari, A. Thiel, F. Ferrer, I. Woelfel, J. C. Chang, A. P. Darold, and A. A. Holland (2020), The Oklahoma Geological Survey Statewide Seismic Network, Seismol. Res. Lett., 91 (2A): 611–621, doi:10.1785/0220190211. Accessed via http://www.ou.edu/ogs/research/earthquakes/catalogs on April 7, 2020.

Weingarten, M., Ge., S., Godt, J. W., Bekins, B. A., and Rubinstein, J, L., 2015. High-rate injection is associated with the increase in U.S. mid-continent seismicity. Science, vol. 348, p. 1336-1340.

Yeck, W. L., Weingarten, M., Benz, H. M., McNamara, D. E., Bergman, E. A., Herrmann, R. B., Rubinstein, J. L., and Earle, P. S., 2016. Far-field pressurization likely caused on the largest injection induced earthquakes by reactivating a large preexisting basement fault structure. Geophysical Research Letters, vol. 43, p. 1-10.

Yehya, A., Yang, Z., and Rice, J. R., 2018. Effect of fault architecture and permeability evolution on response to fluid injection. Journal of Geosphysical Research: Solid Earth, v. 123, p. 9982-9997.

Ying, F., Toran, L., and Schlische, R. W., 2007. Groundwater flow and groundwater-stream interaction in fractured and dipping sedimentary rocks: insights from numerical models.

Zeller, D.E.; Jewett, J.M.; Bayne, C.K.; Goebel, E.D.; O'Connor, H.G.; and Swineford, A. (1968). "The Stratigraphic Succession in Kansas." Kansas Geological Survey Bulletin 189.

Zhai, G., Shirzaei, M., Manga, M., and Chen, X., 2020. Pore-pressure diffusion, enhanced by poroelastic stresses, controls induced seismicity in Oklahoma. PNAS, vol. 116, no. 33, p. 16228-16233.

Zhang, Y., Person, M., Rupp, J., Ellet, K., Celia, M. A., Gable, C. W., Bowen, B., Evans, J., Bandilla, K., Mozley, P., Dewers, T., and Elliot, T., 2013. Hydrogeologic controls on induced seismicity in crystalline basement rocks due to fluid injection into basal reservoirs. Groundwater, vol. 51, no. 4, p. 525-538.

APPENDICES

Appendix A: Code Selection

Numerical Modeling is performed with the TOUGH3 code (Jung et al., 2017) compiled with the EOS7 module, which simulates multiphase, nonisothermal transport of mixtures of pure water and brine (Pruess et al. 2012). TOUGH is an integrated finite difference (Narasimhan et al., 1976) code that solves mass and energy balances for fluid flow in porous media. The general form of this equation is

$$\frac{d}{dt}\int_{V_n} M^\kappa dV_n = \frac{d}{dt}\int_{\Gamma_n} \mathbf{F}^\kappa dV_n \bullet \mathbf{n} d\Gamma_n + \int_{V_n} q^\kappa dV_n \quad (1)$$

where the left-hand side (LHS) is the accumulation term and the right-hand side (RHS) is the flux term. In Equation 1, V_n represents a closed subvolume within the system M represents a mass or energy component (denoted by κ), **F** is mass or heat flux, and q is a sources or sinks. For the model developed here, q represents either injection wells or the basal heat flux. Following Gauss' Divergence Theorem, V_n is bounded by the closed surface Γ_n and **n** is the vector normal to surface area bounding V_n. In TOUGH3, the mass accumulation term, M^κ, is

$$M^\kappa = \Phi \sum S\rho X^\kappa \quad (2)$$

where Φ is porosity, and the mass component M^κ is equal to the sum of the saturation (S), density (ρ), and mass fraction (X). Although TOUGH3 can simulate unsaturated porous media, the present study considers only fully saturated conditions. In Equation 1, the heat accumulation term is, calculated as

$$M^{\kappa+1} = (1-\Phi)\rho_R C_R T + \Phi \sum S\rho u \quad (3)$$

where ρ_R is rock density, C_R is rock specific heat, T is temperature, and u is specific internal energy. Advective mass flux is

$$\sum X^{\kappa}\mathbf{F} \tag{4}$$

with component fluxes calculated via an adaptation of Darcy's Law:

$$\mathbf{F} = \rho\mathbf{u} = -k\frac{k_r\rho}{\mu}(\nabla P - \rho\mathbf{g}) \tag{5}$$

where $\mathbf{u}$ is Darcy velocity, k is absolute (intrinsic) permeability, k_r is relative permeability (not used here, as only aqueous phase fluids are considered), μ is dynamic viscosity, $\mathbf{g}$ is the gravitational acceleration vector, and P is fluid pressure. The TOUGH3 code simulates mass transport via diffusion and hydrodynamic dispersion according to

$$\mathbf{F}^{\kappa}\big|_{dis} = -\sum p\bar{\mathbf{D}}^{\kappa}\nabla X^{\kappa} \tag{6}$$

Where the hydrodynamic dispersion tensor is calculated as

$$\bar{\mathbf{D}}^{\kappa} = D_T^{\kappa}\bar{\mathbf{I}} + \frac{(D_L^{\kappa} - D_T^{\kappa})}{u^2}\mathbf{uu} \tag{7}$$

and longitudinal and transverse dispersivity are given by D_L^{κ} and D_T^{κ}, respectively:

$$D_L^{\kappa} = \Phi\tau_o\tau d^{\kappa} + \alpha_L u \tag{8}$$

$$D_T^{\kappa} = \Phi\tau_o\tau d^{\kappa} + \alpha_T u \tag{9}$$

where d^{κ} is the molecular diffusion coefficient, $\tau_o\tau$ is a tortuosity factor (not considered here, thus assumed unity), and α_L and α_T are longitudinal and transverse dispersivities. The heat flux formulation accounts for both conduction and advection, as given by

$$\mathbf{F} = -\lambda\nabla T + \sum h\mathbf{F} \tag{10}$$

where λ is thermal conductivity and h is specific enthalpy. Variable fluid density is modeled as a mixture of pure water and brine using an end-member mixing model,

$$\frac{1}{\rho_m} = \frac{1 - X_b}{\rho_w} + \frac{X_b}{\rho_b} \tag{4}$$

where X_b is brine mass fraction, ρ_m is the density of the water-brine mixture, ρ_w is the density of pure water, and ρ_b is the brine reference density. The mixture viscosity is modeled as a function of

pressure (P), temperature (T), and composition (X_b).The above governing equations are discretized in space and time using an integral finite difference method for a fully-implicit, backwards finite differencing to solve for a coupled set of nonlinear algebraic equations using Newton-Rhapson (NR) iteration. Iteration is continued until a preset convergence tolerance, here set to 10^{-6}, is achieved. During NR iterations, the time step doubles upon successful convergence within four iterations and halves if unsuccessful within eight iterations.

Appendix B: Simulation Results (5 km bmsl)

Scenario A: Impermeable NFZ

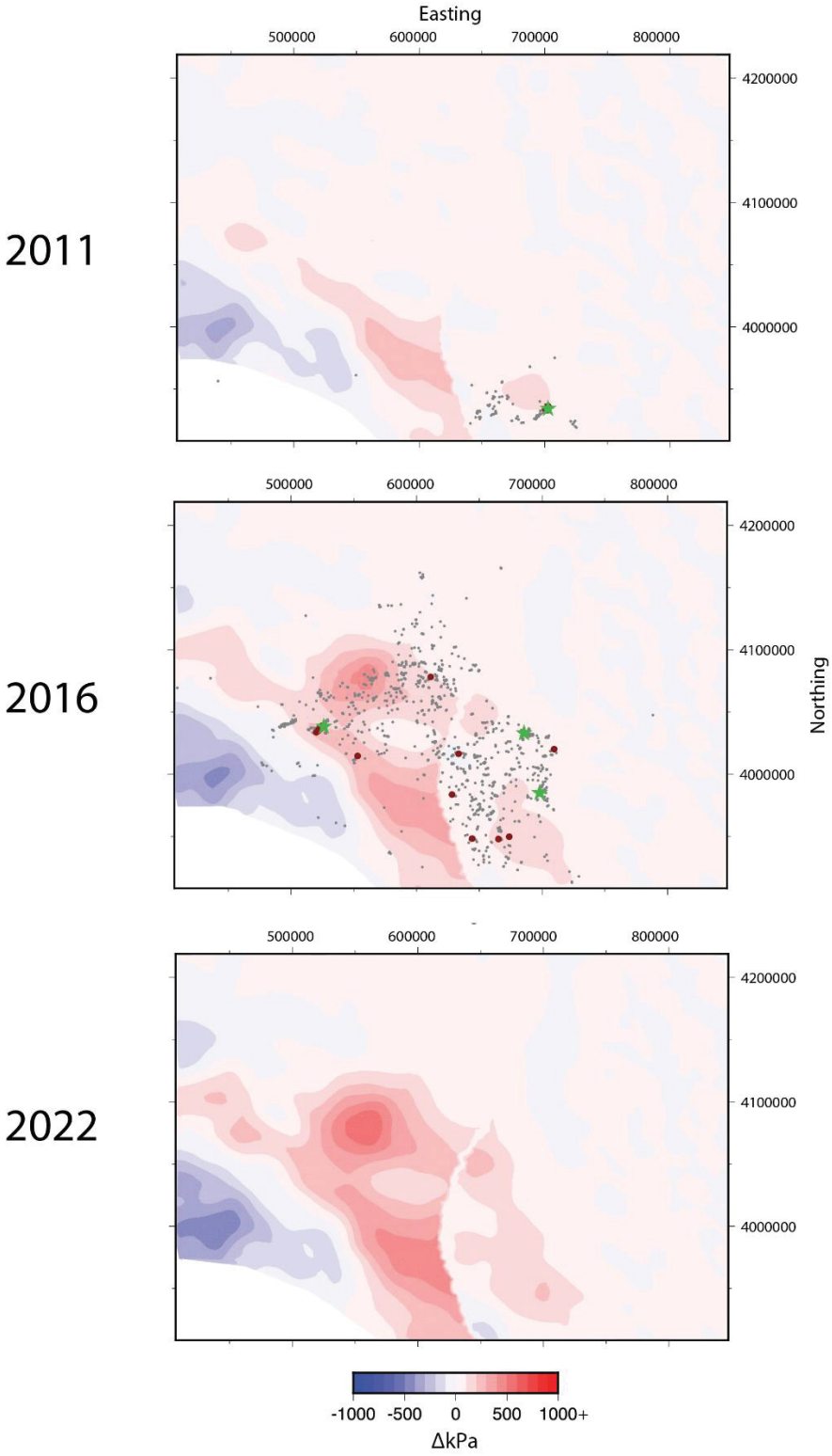

Scenario B: Low-Permeability, Isotropic NFZ

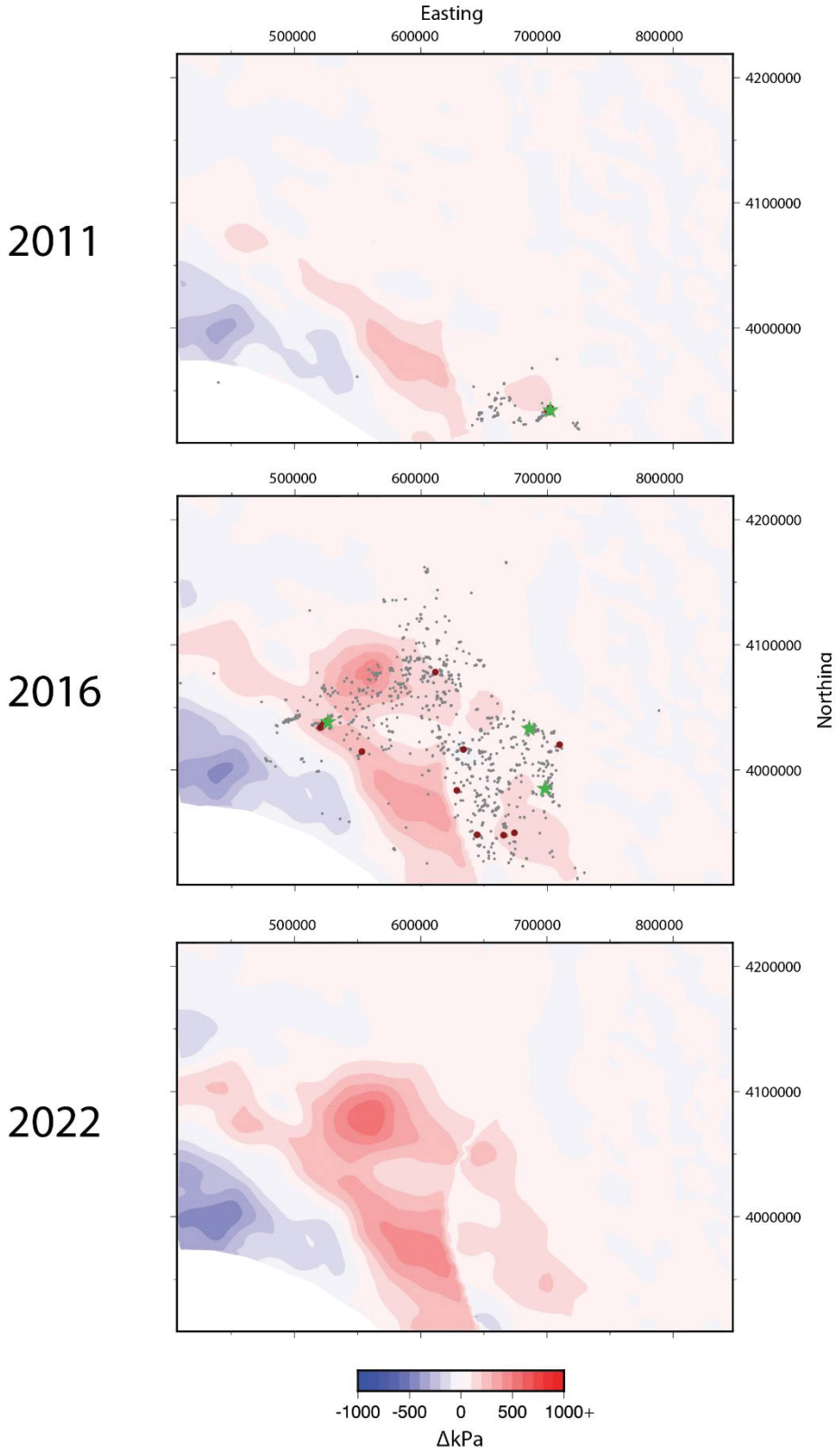

Scenario C: Anisotropic NFZ

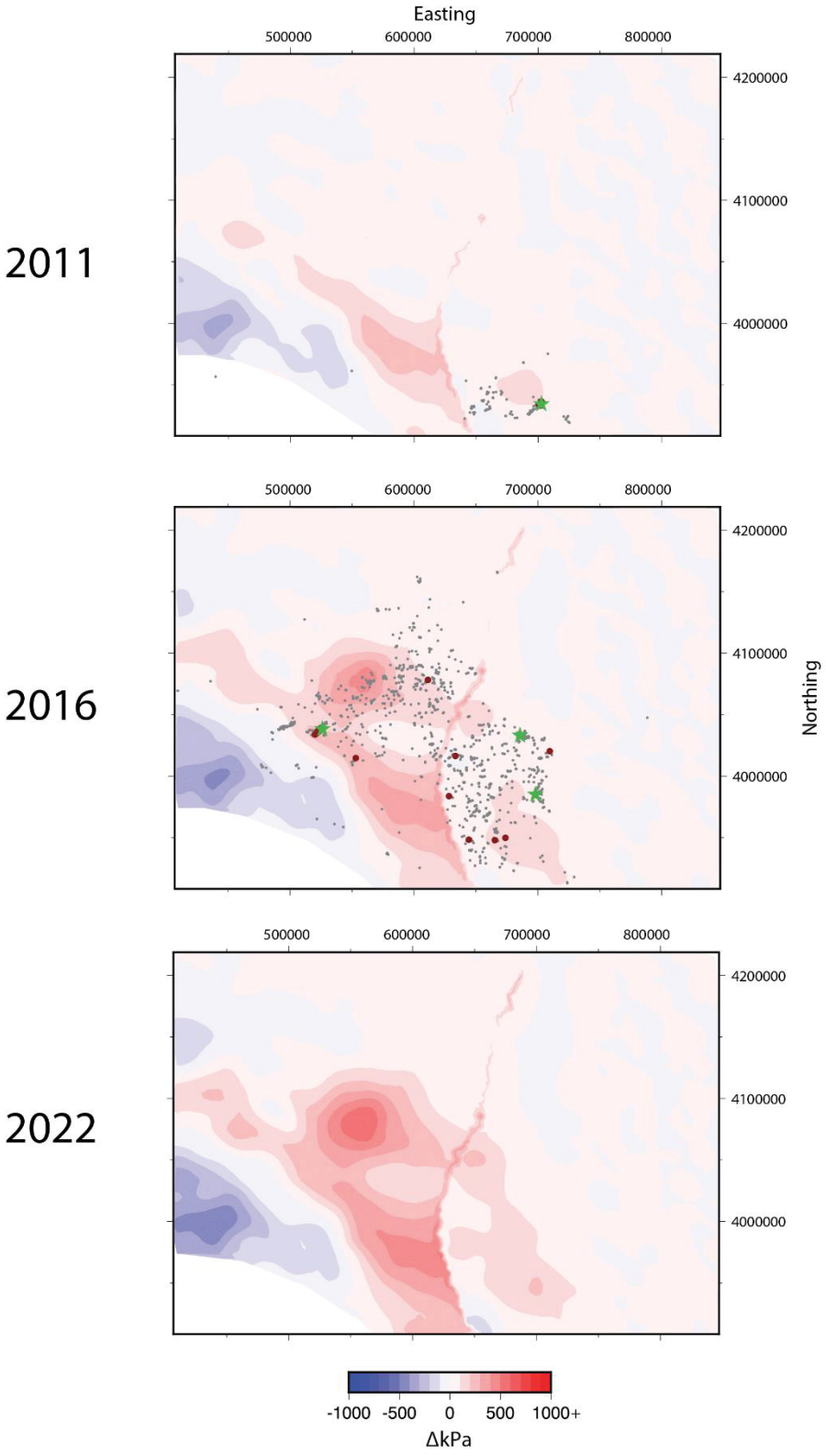

Scenario D: High-Permeability Basement

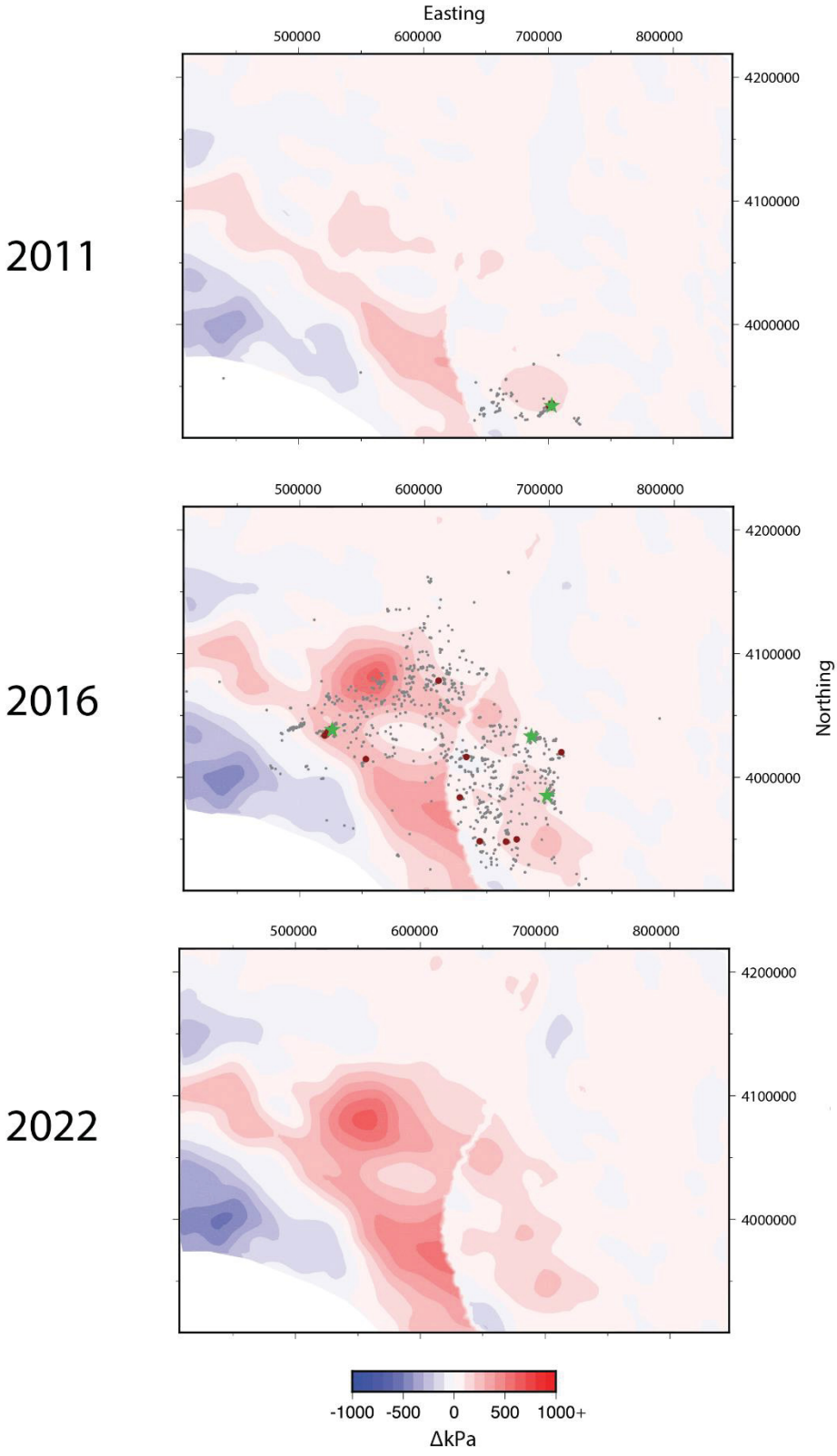

Scenario E: Low-Permeability Basement